ORNL/TM-2022/2691/V8

Volume 8: Epithermal and Fast Neutron Radiography Facility

HFIR Futures – Enhanced Capabilities Series

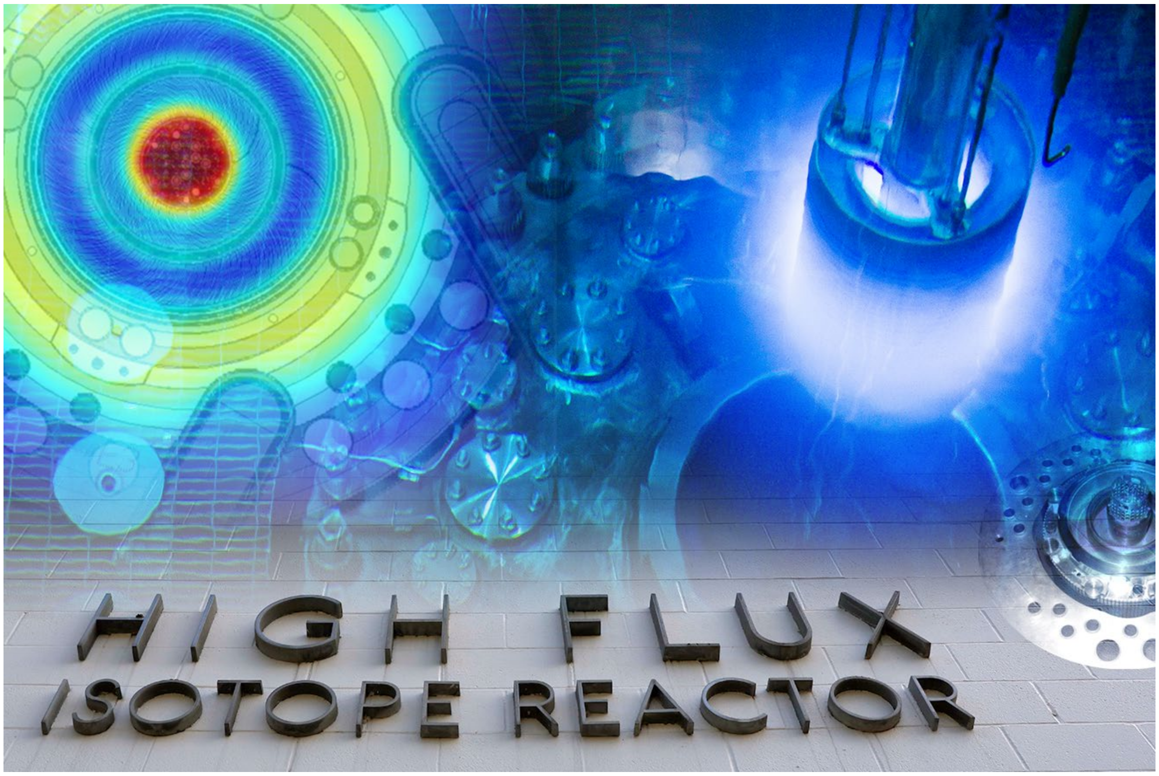

Padhraic L. Mulligan
Matthew J. Frost
Zain Karriem
Jonathan R. Chappell
Jason M. Harp

September 2023

ORNL IS MANAGED BY UT-BATTELLE LLC FOR THE US DEPARTMENT OF ENERGY

ORNL/TM-2022/2691/V8

Nuclear Energy and Fuel Cycle Division
Neutron Technologies Division
Radioisotope Science and Technology Division

VOLUME 8: EPITHERMAL AND FAST NEUTRON RADIOGRAPHY FACILITY HFIR FUTURES – ENHANCED CAPABILITIES SERIES

Padhraic L. Mulligan
Matthew J. Frost
Zain Karriem
Jonathan R. Chappell
Jason M. Harp

September 2023

Prepared by
OAK RIDGE NATIONAL LABORATORY
Oak Ridge, TN 37831
managed by
UT-BATTELLE LLC
for the
US DEPARTMENT OF ENERGY
under contract DE-AC05-00OR22725

CONTENTS

LIST OF FIGURES

LIST OF TABLES

ACKNOWLEDGMENTS

This research is sponsored by the Laboratory Directed Research and Development Program of Oak Ridge National Laboratory, managed by UT-Battelle, LLC, for the US Department of Energy under contract DE-AC05-00OR22725. The authors acknowledge and thank Joel McDuffee, Chris Bryan, Hassina Bilheux, and Ken Littrell for thoughtful discussions during the conceptual stage of this working group. The authors would also like to acknowledge Rose Raney and Jacob Gorton of Oak Ridge National Laboratory for their comprehensive technical reviews of this paper.

ABBREVIATIONS

ADVANTG	Automated Variance Reduction Generator
ANNRI	Accurate Neutron–Nucleus Reaction Measurement Instrument
BESAC	Basic Energy Sciences Advisory Committee
BRR	Budapest Research Reactor
CAD	computer-aided design
CCD	charge-coupled device
CUPI^{2}D	Complex, Unique and Powerful Imaging Instrument for Dynamics
DOE	US Department of Energy
ERNI	Energy Resolved Neutron Imaging
ERS	East Radiography Station
FP5	Flight Path 5
FTS	First Target Station
HEU	highly enriched uranium
HFEF	Hot Fuel Examination Facility
HFIR	High Flux Isotope Reactor
HFIRCON	High Flux Isotope Reactor Controller
INL	Idaho National Laboratory
J-PARC	Japan Proton Accelerator Research Complex
LANSCE	Manuel Lujan Neutron Scattering Center of the Los Alamos Neutron Science Center
LAVAMINT	LAVA Model Interrogator
L/D	length-over-diameter
LDRD	Laboratory Directed Research and Development
LEU	low-enriched uranium
MCNP	Monte Carlo N-Particle
MLF	Materials and Life Science Experimental Facility
MURR	University of Missouri Research Reactor
NECTAR	Neutron Computed Tomography and Radiography
NEUTRA	Neutron Transmission Radiography [thermal neutron imaging facility]
NMC&A	nuclear material controls and accountability
NOBORU	Neutron Beam Line for Observational Research Use
NRAD	Neutron Radiography [reactor]
ORIGEN	Oak Ridge Isotope Generation
ORNL	Oak Ridge National Laboratory
ORNL-TN/MCNP5	ORNL-Transformative Neutronics/MCNP5
PNI	polarized neutron imaging
PSI-SINQ	Paul Scherrer Institute Spallation Neutron Source
QMNB	Quasi-Monoenergetic Neutron Beams
RADEN	neutron radiography (Energy-Resolved Neutron Imaging System)
RPV	reactor pressure vessel
SANS	small angle neutron scattering
SENSe	Sustaining and Enhancing Nuclear Science
SNS	Spallation Neutron Source
STS	Second Target Station
TOF	time-of-flight
VXF	vertical experiment position

ABSTRACT

The Sustaining and Enhancing Nuclear Science Initiative at Oak Ridge National Laboratory (ORNL) was created to explore potential enhancements to scientific capabilities in the High Flux Isotope Reactor as part of a reactor pressure vessel replacement project. One proposed scientific enhancement included creation of an epithermal and fast neutron radiography station on the HB-3 beam tube with the capability to image highly radioactive specimens such as irradiated nuclear fuel rods, isotope production targets, or spallation neutron target materials. This document summarizes findings and recommendations from a working group of ORNL staff tasked with conceptualizing such a facility and includes a background of similar instruments at other research facilities, technical specifications, and an estimate of procurement cost and schedule.

1. INTRODUCTION

Notably missing from the existing and planned imaging capabilities at Oak Ridge National Laboratory (ORNL) is an epithermal (0.3 eV–10 keV) and fast (10 keV–20 MeV) neutron imaging facility. This type of facility can image materials that cannot be imaged using thermal (0.025 eV) neutrons with any amount of sensitivity. Examples include nuclear fuel assemblies, which typically comprise actinides with very large thermal neutron absorption cross sections. Performing radiography of such materials with thicknesses of more than a few millimeters would prove to be challenging with thermal or cold neutrons. Furthermore, it is likely that these types of materials have already been processed, irradiated, and tested at ORNL. Having a facility near the handling areas designated for highly activated materials would simplify transportation and would enable quick determination of irradiation effects for a variety of materials. This report summarizes the efforts of a working group tasked with conceptualizing an epithermal and fast neutron imaging facility as part of the High Flux Isotope Reactor (HFIR) Sustaining and Enhancing Nuclear Science (SENSe) Initiative.

1.1 BACKGROUND OF THE HFIR 2100 SERIES REPORTS

In 2020, the US Department of Energy (DOE) Office of Science chartered a Basic Energy Sciences Advisory Committee (BESAC) to assess the scientific justification for a domestic high-performance reactor–based research facility. This committee delivered a report with specific recommendations to continue operations beyond the year 2100, thus enabling future additional scientific capabilities and conversion to low-enriched uranium (LEU) (Birgeneau, Clark et al. 2020). The review determined that HFIR will have a critical role in the future of US neutron science research, and the report recommends the immediate pursuit of scientific enabling enhancements, including reactor pressure vessel (RPV) replacement, conversion to LEU fuel, enhanced capabilities for in-core irradiations and neutron scattering research, fuel assembly modifications, and restoration of the flux intensity of the original 100 MW highly enriched uranium (HEU) operations.

In response to the BESAC report, an ORNL-funded initiative was established to critically assess the hardware, systems, and infrastructure required to sustain and enhance HFIR capabilities. The HFIR-Sustaining and Enhancing Neutron Science (SENSe) initiative consists of three Laboratory Directed Research and Development (LDRD) projects assessing (1) infrastructure-enabling operation past 2100, (2) non–neutron-scattering scientific capability enhancements and planning, and (3) neutron scattering scientific capability enhancements and planning. Bryan and Chandler (2022) provide more information regarding HFIR, the BESAC report recommendations, the HFIR-SENSe Initiative, and the goals of the three LDRD projects.

The effort to brainstorm non-scattering scientific enhancements at HFIR was a "blue-sky" engagement with researchers across ORNL and has yielded both incremental improvement ideas, as well as new transformational capabilities. In this effort, 35 concepts were grouped into 13 separate working groups to further develop the concepts, build a scientific justification, identify potential sponsors, and estimate costs and schedules for each concept. This effort culminated in this multivolume series summarizing these efforts and ideas. Table 1-1 itemizes the volumes.

Table 1-1. Summary of the HFIR 2100 Series

Volume	Report number	Volume title
1	ORNL/TM-2022/2691/V1	Volume 1: Introduction to the HFIR Futures — Enhanced Capabilities Series
2	ORNL/TM-2022/2691/V2	Volume 2: Hot Cells Connected to the Reactor Pool
3	ORNL/TM-2022/2691/V3	Volume 3: Online Insertion and Removal Facilities
4	ORNL/TM-2022/2691/V4	Volume 4: Detection Systems and Ultra-Cold Neutrons
5	ORNL/TM-2022/2691/V5	Volume 5: Flexible Flux Trap Configurations
6	ORNL/TM-2022/2691/V6	Volume 6: Experiment Facility Spectrum Tailoring
7	ORNL/TM-2022/2691/V7	Volume 7: Cryogenic Facility
8	ORNL/TM-2022/2691/V8	Volume 8: Epithermal and Fast Neutron Radiography Facility
9	ORNL/TM-2022/2691/V9	Volume 9: Critical Facility
10	ORNL/TM-2022/2691/V10	Volume 10: Flow Test Facilities
11	ORNL/TM-2022/2691/V11	Volume 11: Modeling & Simulation
12	ORNL/TM-2022/2691/V12	Volume 12: Flow Loop Facilities
13	ORNL/TM-2022/2691/V13	Volume 13: Neutrino Facilities

1.2 DESCRIPTION OF WORKING GROUP

The working group was composed of ORNL staff members from multiple divisions, including the Nuclear Energy and Fuel Cycle Division, Neutron Technologies Division, Radioisotope Science and Technology Division, and the Neutron Scattering Division. Virtual meetings were held biweekly to discuss and present research and modeling progress.

1.3 SIGNIFICANCE OF WORKING GROUP

The HFIR SENSe initiative presents a unique, transformative opportunity to expand the scientific research capabilities currently available at the laboratory. Epithermal and fast neutron radiography were identified capabilities missing from the ORNL research portfolio that would benefit several current programs. Neutron imaging is a complementary technique to x-ray imaging, in the sense that x-rays are highly attenuated by heavier (high-Z) materials, whereas neutrons are scattered or attenuated more significantly by light (low-Z) materials. Epithermal or fast neutron radiography is particularly useful because it enables imaging of mixed high-z/low-z materials without significant attenuation while providing reasonable contrast as a result of the smaller variability in cross section between elements at higher energies (Zboray, Adams et al. 2017). This working group sought to conceptualize an epithermal and fast neutron radiography facility by repurposing the HB-3 beam tube. Adding this capability will have significant benefits for several key DOE initiatives, including the Advanced Fuels Campaign for imaging radioactive fuel, the DOE Isotopes program for imaging irradiated isotope targets, and the DOE Office of

Science investigation of Spallation Neutron Source (SNS) spallation target materials. The group compiled information on existing epithermal and fast neutron beam facilities and beam filtering techniques, along with detailed physics-based modeling of a concept beam imaging station. The team also researched logistical and safety constraints involved with transporting highly radioactive specimens from the HFIR pool-top to the radiography instrument on the ground floor.

1.4 NEUTRON RADIOGRAPHY AT ORNL

Neutron radiography is currently used at beamline CG1D (Santodonato, Bilheux et al. 2015) in the Cold Guide Hall at HFIR. The instrument uses a cold neutron beam flux to analyze attenuation in materials, as well as some neutron wavelength–resolved attenuation effects with resolutions $\Delta\lambda/\lambda$ of 10% or <1%, depending on the setup. Polarized neutron imaging (PNI) has also been used to resolve integrated magnetic fields as small as 4×10^{-5} T· m (Dhiman, Ziesche et al. 2017). The setup is versatile and has been a valuable asset in developing neutron radiography as a world-class capability at ORNL.

The result of those developments has been a series of proposed and under-construction installation projects that will provide ORNL with a range of world-class neutron radiography capabilities. Specifically, VENUS is under construction at the SNS First Target Station (FTS) located on beamline 10. VENUS will have a time-of-flight (TOF) resolution capability permitting visualization of very well–resolved Bragg-edge images, thus contributing critical data toward a wide range of science disciplines (Bilheux, Herwig et al. 2015). Furthermore, the proposed Second Target Station (STS) project will include a high-intensity, fast-imaging instrument as one of its initial developments. The Complex, Unique and Powerful Imaging Instrument for Dynamics (CUPI^{2}D) will provide high imaging resolution in both time and wavelength to quantify fast dynamics of materials in-situ with spatial resolution on the order of 50 microns. This capability is critical for bridging the gap between traditional real-scale imaging and *q* resolved reciprocal space structure features of materials, where small angle neutron scattering (SANS) is the usual instrument of choice. An imaging instrument capable of radiography by epithermal and faster neutron fluxes are notably missing from this list.

2. STATE OF THE ART FAST NEUTRON BEAM FILTERING TECHNIQUES AND USER FACILITIES

Neutron imaging has been a critical scientific technique for performing radiography and tomography of objects, dating back to 1935 when the first neutron radiography was performed using a Ra/Be source (Lehmann, Vontobel et al. 2011). This technique remains very active to this day, with most large neutron generation facilities (reactors and spallation sources) having some neutron radiography capability. Although cold or thermal beams are typically the most common energy spectra for neutron imaging, several facilities exist worldwide with epithermal or fast neutron beams. Higher energy (eV to MeV) neutrons are also more effective for imaging mixed media with high- and low-Z material such as UO_2, NpO_2, and UC without significant beam starvation or loss of contrast (Zboray, Adams et al. 2017). The following sections provide an overview of the state of the art for producing fast and epithermal neutron beams using various materials as bandpass filters. A brief discussion of existing fast and epithermal beam facilities is also included to provide a basis for comparing the proposed HFIR beamline.

2.1 NEUTRON BEAM FILTERING TECHNIQUES AND MATERIALS

Neutron beam facilities generally receive neutron flux from one of two physical processes: reactor-based fission of transuranic materials, or accelerator-based spallation of heavy metals. Both processes generate neutrons of high energy which are typically slowed down or moderated to energies more suitable for detection or investigating sample structures and compositions. Neutrons generated via fission are produced with average kinetic energy on the order of 2 MeV, while spalled neutrons cover a range of energies up to tens of MeV. This moderation process can create a spectrum of neutron energies which requires additional filtering to create a low-pass or narrow-band pass filter. Although neutron beams can also be generated through other mechanisms, including spontaneous fission (^{252}Cf), fusion reactions ($D + T \rightarrow \ ^{4}He + n$ and $D + D \rightarrow \ ^{3}He + n$), alpha neutron sources (^{241}Am-Be), and gamma neutron sources (^{9}Be, γ or D, γ), these are beyond the scope of this document and are not reviewed here. This section provides several approaches for neutron filtering techniques.

2.1.1 Experimental Filtering Techniques

The Accurate Neutron–Nucleus Reaction Measurement Instrument (ANNRI), located at the Materials and Life Science Experimental Facility (MLF) of the Japan Proton Accelerator Research Complex (J-PARC) explored Fe and Si in natural isotopic abundancies to produce quasi-monoenergetic neutron peaks in the keV range (Rovira, Kimura et al. 2021). Filters with varying thicknesses made of natural Fe and Si placed in the rotary collimator of the facility produced neutron peaks with centroids of 23.5, 51.5, and 122.7 keV. Similar filters were used to produce 24 and 144 keV quasi-monoenergetic beams using Fe and Si, respectively, at the University of Missouri Research Reactor (MURR) Facility (Tsang and Brugger 1976) for a continuous neutron beam. Other combinations of Pb, Al, and S filters, in conjunction with Si and Fe, were experimentally measured and shown to achieve a peak flux of 2.5×10^{6} n cm^{-2} s^{-1} for 144 keV (28 keV FWHM) neutrons and 1.2×10^{6} n cm^{-2} s^{-1} for 24 keV (1.8 keV FWHM) neutrons. Single-crystal Bi and Si filters have been used experimentally (Aizawa, Matsumoto et al. 1986) at the Musashi reactor (decommissioned) as a gamma and fast neutron filter concept for thermal beamlines, demonstrating that a combination of 10 cm Bi with 21 cm Si is an effective band-pass filter for thermal neutrons and gamma attenuation. A rotational collimator was used at the High Flux Beam Reactor (decommissioned) with Fe and Sc to select quasi-monoenergetic neutron beams of 2 and 24 keV, respectively, with reduced gamma ray and thermal neutron transmission (Greenwood and Chrien 1976). Depleted ^{238}U has also been used as a neutron filter at the Rensselaer Polytechnic Institute electron linear accelerator to produce approximately 30 discrete energy peaks ranging from 34 eV to 6.2 MeV (Moreh, Block et al. 2006).

2.1.2 Modeled and Theoretical Filtering Techniques

Advances in modeling techniques for neutron beam filters have enabled analysis of several less common materials under a variety of crystalline and thermal conditions. A semi-empirical formula for thermal diffuse (inelastic) scattering cross sections for a variety of materials was developed (Freund 1983) to predict filter efficacy for neutron energies up to 10 eV. Freund investigated a variety of materials, including Si, Cu, Bi, Al_2O_3, and Be, but did not perform optimization studies with these filters. Although the focus was primarily to optimize filters for thermal neutron beams, the same technique could be utilized to optimize filters for higher energy beams. Adib et al. (2002) provided a generalized formula for Bragg scattering in poly- and monocrystalline neutron filters. This work showed that a 10 cm thick single crystal (111) of lead cooled to liquid nitrogen temperatures was effective as a thermal neutron filter with low gamma background. Polycrystalline lead was shown to be an effective gamma and neutron filter for cold (0.5 nm) neutron beams. Numerical estimates, along with comparisons to experimental measurements, were extended by Adib et al. (2015) to include BeO and SiO_2, finding that 25 cm of polycrystalline BeO_2 cooled to 77 K is an effective filter for removing epithermal and fast neutrons. Similar efficacy can be found using 50 cm of polycrystalline SiO_2, although with slightly lower beam intensity. The Quasi-Monoenergetic Neutron Beams (QMNB) code was developed to explore a range of filter materials and thicknesses to achieve optimal configurations for near monoenergetic neutron beam filters from 1–133 keV (Mansy, Bashter et al. 2015). The code determined 9 peaks within this energy range while maximizing beam purity and flux. MgF_2 and BeF_2 were analyzed by Al-Qasir (Al-Qasir and Qteish 2017) and found to be a highly effective fast neutron filter, more so than the more commonly used MgO and sapphire materials.

2.2 EXISTING FACILITIES

While thermal spectra are arguably the most common neutron beam facilities, followed by cold neutron beams, several epithermal or variable energy beamlines exist around the globe. The following sections provide an overview of operational fast and epithermal neutron beam facilities from reactor and pulsed neutron sources. This list is not exhaustive and does not include facilities which have been decommissioned, but it is intended to provide a baseline for the current state of the art in fast and epithermal neutron beam facilities. This review also includes two facilities with thermal beamlines designed specifically for imaging highly radioactive materials.

2.2.1 Reactor Based Epithermal and Fast Imaging Facilities

2.2.1.1 Neutron Radiography (NRAD) Reactor

The Neutron Radiography (NRAD) reactor, located at the Idaho National Laboratory (INL) in Idaho Falls, Idaho, is home to two neutron radiography stations that are used to examine highly radioactive samples (Craft, Wachs et al. 2015). The NRAD East Radiography Station (ERS) is operational and can receive irradiated fuel samples from the INL Hot Fuel Examination Facility (HFEF), which is situated in the same building directly above the NRAD reactor. Radioactive samples are transported from the HFEF main cell into the NRAD East Beam using a remotely operated elevator. The ERS facility can select one of three boron nitride apertures at diameters of 8.89, 3.53, and 1.47 cm to achieve length-over-diameter ratios (L/D) of 50, 125, or 300. Imaging is performed using indirect transfer foil cassettes located 444.5 cm from the beam aperture. The field of view at the imaging location is 17.8 × 43.2 cm and receives a thermal neutron flux of 9.61×10^{6} n cm^{-2} s^{-1} with a cadmium ratio of 2.05 (Giegel, Craft et al. 2021).

Due to the very high gamma dose rate produced by fuel specimens in the ERS facility (10^{2} – 10^{4} Gy/hr) (Craft, Wachs et al. 2015), neutron imaging is limited to techniques which are resistant to intense gamma radiation. The ERS uses an indirect foil film transfer radiography technique which places two thin sheets of Dy and In behind the sample under investigation. A thin sheet of Cd is placed between the two activation foils (with Dy located closest to the sample) to absorb thermal neutrons, utilizing the large capture resonance of In (1.46 eV) to perform epithermal neutron images. Foils are exposed 22 minutes for an image capture and are subsequently placed in contact with x-ray film overnight. Films are developed using an automated Kodak film processor and digitized with a nominal 21 μm pixel pitch. Although this method is effective for producing radiographs in extremely high gamma fields, it can also be quite slow, requiring 1–2 days to develop an image.

2.2.1.2 Heinz Maier-Leibnitz Zentrum: FRM-II

The Heinz Maier-Leibnitz Zentrum reactor FRM-II is a 20 MW research reactor near Garching, Germany and is used for a variety of neutron beam, in-core irradiation, and isotope production efforts. It contains 12 beam tube facilities to serve more than 25 instruments, including the Neutron Computed Tomography and Radiography (NECTAR) station on beam tube SR10. NECTAR uses a converter facility at the beam entrance that is composed of two plates of HEU to produce fission spectrum neutrons with a mean energy of 1.8 MeV with flux values between 8.7×10^{5} – 4.7×10^{7} n cm^{-2} s^{-1} (Bucherl and Sollardl 2015). A 1 cm thick B_4C filter suppresses thermal neutrons, while a 1 cm Pb filter is used for gamma reduction (Bücherl, Lierse von Gostomski et al. 2011). Additional filters of Fe, Cd, and Pb with a 2.47 cm beam diameter are also used for additional gamma and thermal neutron reduction. Beam collimation values are ≤233, and imaging is primarily performed using a charge-coupled device (CCD) detection system coupled to a ZnS scintillation screen, although neutron-sensitive imaging plates can also be used.

2.2.1.3 Budapest Neutron Centre

The Budapest Research Reactor (BRR) is a 10 MW research reactor on the Budapest Neutron Centre campus in Budapest, Hungary. The BRR contains approximately 40 vertical irradiation facilities, as well as 8 radial and 2 tangential beam ports, with a variety of neutron scattering, diffraction, and detection instruments (Tozser 2009). Aa thermal beamline at the facility was recently modified for fast neutron imaging capabilities by adding a 10 mm thick borated rubber mat and 300 mm of lead to suppress thermal neutrons and gammas, respectively (Zboray, Adams et al. 2017). The addition of these filtering materials reduced the fast flux from 2.7×10^7 n cm^{-2} s^{-1} to 3.7×10^4 n cm^{-2} s^{-1} (E> 2.8 MeV), which was calculated using the ^{58}Ni activation method. The beam exiting the primary aperture has a circular geometry 28 mm in diameter and an L/D of 165 at the imaging detector. Imaging was performed on a variety of specimens using a low-cost TS14-cooled CCD camera focused on an 8 mm thick St. Gobain BC400 plastic scintillator converter plate. This setup achieved a spatial resolution of 1.3 mm with approximately 10 minutes of exposure time. Gammas in the beam were estimated to account for ~1% of signals in the imaging system, and some degradation was observed in the CCD after long exposure times. Recommendations for improving the facility included using a ZnS(Ag) plastic scintillator with greater light yield, additional gamma suppression filters, and customized shielding for the CCD camera to reduce cumulative damage effects.

2.2.1.4 Ohio State University Research Reactor

The Ohio State University Research Reactor in Columbus, Ohio, is a 500 kW pool-type light-water research reactor that is used for various teaching and research purposes. The reactor contains several in-core irradiation facilities and two beam ports for a variety of neutron instrumentation, including neutron depth profiling (Mulligan, Cao et al. 2012), neutron radiography, and neutron tomography. The fast neutron beam facility is composed of a series of graphite, Pb, borated Al, and high-density polyethylene collimation disks, with a solid disk of Bi for gamma suppression (Ibrahim, Matthew Van et al. 2020). At the collimator exit, the neutron beam is 32 mm in diameter, with an L/D ratio of 62. Monte Carlo N-Particle (MCNP) modeling estimated that the fast (1.6 MeV) flux at the collimator exit was 5.4×10^7 n cm^{-2} s^{-1} with a comparable thermal neutron flux and a non-negligible gamma component. Experimental measurements of the neutron spectrum and peak fast flux are planned.

2.2.2 Accelerator Based Epithermal and Fast Imaging Facilities

2.2.2.1 Paul Scherrer Institute Spallation Neutron Source (PSI-SINQ)

The SINQ spallation neutron source (Bauer 1998) at the Paul Scherrer Institute in Würenlingen, Switzerland, is a steady-state neutron source used for a variety of neutron scattering, reflectometry, and imaging instruments. SINQ produces neutrons using a high-energy (590 MeV) proton beam impinging upon a Zircaloy rod target or a lead target clad in stainless steel and/or Zircaloy. The SINQ thermal neutron imaging facility, Neutron Transmission Radiography (NEUTRA), which often handles nonradioactive specimens, was modified to accommodate additional shielding and remote handling of highly radioactive materials with dose rates of 10 Sv/hr such as irradiated nuclear fuel (Groeschel, Schleuniger et al. 1999) and spallation targets in SINQ (Lehmann, Vontobel et al. 2004, Vontobel, Tamaki et al. 2006). This modified facility, named NEURAP, consists of a 28 cm beam and an imaging plate 40 mm wide by 250 mm tall (Vontobel, Tamaki et al. 2006). The facility is capable of coarse tomography (15° rotational increments) and has been used to identify ZrH_2 formations in SINQ spallation targets (Vontobel, Tamaki et al. 2006). For highly radioactive target materials with strong gamma emissions, the NEURAP facility performs imaging via two indirect exposure processes. In the converter method, a Dy foil is first placed in the beam to capture neutron transmissions through the sample and is subsequently removed from the beam and placed in contact with a secondary detector sensitive to beta and gamma emissions from the activated Dy foil. The Dy or In foil undergo exposure times of approximately 3 minutes in the neutron beam, after which the Dy foil is in contact with an imaging plate (Lehmann, Vontobel et al. 2004) for 30–180 minutes. A second track-etch method uses neutron-induced (n, α) reactions from ^{10}B to produce tracks in a nitro cellulose sheet. The sheet is exposed for 15 minutes, which is followed by a 20-minute etch (Lehmann, Vontobel et al. 2004). CCD imaging is also available at the facility. The facility contains three locations for imaging, the locations of which range from 6.4 to 13.1 m from the target center (Groeschel, Schleuniger et al. 1999). Beam collimation values (L/D) range from 200–550, with neutron flux ranging from $1.6\times10^7 – 3.0\times10^6$ n cm^{-2} s^{-1} (Groeschel, Schleuniger et al. 1999). The facility is capable of handling irradiated fuel elements that are 70 cm in length and 10.8 mm in diameter.

2.2.3 Japan Proton Accelerator Research Complex, Materials and Life Sciences Experimental Facility (J-PARC, MLF)

J-PARC is a pulsed spallation neutron source located in Ibaraki Prefecture, Japan, with 23 beam ports and more than 20 neutron instruments serving a variety of neutron scattering and detection needs (Ikeda 2009). Neutrons are generated from a rectangular 3 GeV double-pulsed proton beam impinging upon a liquid mercury target at a frequency of 25 Hz. Spalled neutrons are moderated using liquid hydrogen before traveling to a variety of diffractometer, spectrometer, and reflectometer instruments. Additionally, three higher neutron energy beamlines are used for cross section measurements (ANNRI), neutron detector development (Neutron Beam-line for Observational Research Use (NOBORU)), and neutron radiography (Energy-Resolved Neutron Imaging System (RADEN)). TOF instruments utilizing thermal or cold neutrons from this facility do not need to account for the time structure of the incident proton beam because the time scale of the neutron slowing down process dominates. Deconvolution of the proton beam time structure is necessary for instruments using neutron energies above several eV because the neutron energy and intensity vary with each proton pulse.

Simulation work performed by Kino (Kino, Furusaka et al. 2014) has shown that the energy resolution of the TOF technique with a double pulse beam on the ANNRI instrument deteriorates above 10 eV, which was confirmed experimentally using diffraction and neutron capture resonance measurements in the facility. As mentioned in Section 2.1.1, ANNRI uses filters composed of Si and Fe in a rotary collimator to produce a circular beam 6–22 mm in diameter. ANNRI is primarily used for nuclear structure and cross-section measurements using an array of HPGe and NaI spectroscopic detector clusters (Kenji, Yukinobu et al. 2017).

The NOBORU instrument is another high-energy beamline on BL10 in the MLF which is used to develop and characterize new detectors, as well as concept instruments for the facility. This instrument can provide a high-flux neutron source over a broad energy range, with neutrons energies as high as 10 MeV. The instrument is capable of using several types of filters, including Cd, Ta, In, Cu, borosilicate glass, Pb, and Bi, for individual experiment needs. NOBORU has a beam footprint of 100×100 mm at the sample position and can achieve beam collimation ratios (L/D) ranging between 14- and 1,875.

RADEN is a pulsed neutron imaging instrument on BL22 and is used to perform neutron radiography and tomography measurements. It is capable of performing energy-resolved neutron imaging with a beam area of up to 300×300 mm and spatial resolution on the order of >30 μm with CCD detectors (Shinohara, Kai et al. 2020). Neutron energies are selectable for E > 1.1meV, with L/D values ranging between 180 and 7,500. The instrument is equipped with multiple sample stages with rotational and translations movement capabilities and can hold samples of up to 1,000 kg. The instrument has neutron apertures ranging from 2 to 50.1 mm in diameter. Imaging is performed using a ^{6}LiF/ZnS scintillator coupled to a CCD camera, or through the use of micropattern plate detectors coupled to high-speed field-programmable gate array (FPGA) systems.

Table 2-1. Neutron flux characteristics for high energy beamlines at J-PARC MLF (Kenji, Yukinobu et al. 2017)

Instrument	Facility	Neutron flux, @1 MW ($n\ cm^{-2}\ s^{-1}$)	Neutron energy
ANNARI	J-PARC	4.3×10^7 9.3×10^5 1.0×10^6	$1.5 - 25$ meV $9.0 - 1.1$ eV $0.9 - 1.1$ keV
NOBORU	J-PARC	4.8×10^7 1.2×10^7 1.2×10^6	< 0.4 eV > 1 MeV > 10 MeV
RADEN	J-PARC	1.7×10^7 3.9×10^6 1.1×10^8	< 0.45 eV 1 eV < 1 MeV

2.2.4 Los Alamos Neutron Science Center

The Manuel Lujan Neutron Scattering Center of the Los Alamos Neutron Science Center (LANSCE) in Los Alamos, New Mexico, is a neutron scattering user facility home to four scattering and neutron imaging instruments. LANSCE uses an 800 MeV linear accelerator to produce 300 nanosecond proton pulses in 20 Hz intervals upon a split tungsten target (Tremsin, Vogel et al. 2013). The target can receive 135 µA of proton beam current, generating neutrons in in the cold to hundreds of keV energy range (Lisowski and Schoenberg 2006). The Energy Resolved Neutron Imaging (ERNI) facility on Flight Path 5 (FP5) is equipped to perform energy-resolved neutron resonance spectroscopy, imaging, and tomography on a range of samples. The beamline can be modified to suit specific experiment needs such as those including 5 cm of Pb to suppress prompt gammas generated by the spallation process. Collimation is achieved through a series of steel and CH_2 apertures with a final beam diameter of 0.312 inches (Tremsin, Vogel et al. 2013). Differential neutron flux at the target location is nominally 1.9×10^8 n cm^{-2} s^{-1} eV^{-1} for thermal neutrons and 3.0×10^6 n cm^{-2} s^{-1} eV^{-1} for energies above 1 eV (2022). Beam sizes range from 1 mm to 1 m in diameter, and sample locations are at 6 and 60 m from the spallation source. Imaging at the facility is generally performed using microchannel plate detectors capable of 55×55 µm spatial resolution. The facility has been used to perform isotope density tomographic measurements of irradiated nuclear fuel (Losko and Vogel 2022) using energy resolved neutron imaging, as well as radiography of nuclear fuel assemblies, to determine structural defects such as voids, inclusions, and cracks (Tremsin, Vogel et al. 2013).

3. MODELING AND ANALYSIS OF EPITHERMAL AND FAST NEUTRON RADIOGRAPHY INSTRUMENT

To assess the viability of an epithermal and fast neutron radiography instrument installation at HFIR, a series of calculations were performed. These included neutron and photon transport calculations from the HFIR core to the beam tube entry, ray tracing calculations for a range of aperture diameters and imaging lengths, a simulated radiograph of a prototypical fuel pellet in the proposed facility, and neutron activation calculations for two prototypical irradiation targets to estimate the gamma source strength of a sample imaged in the facility. The following sections provide details of these calculations.

3.1 HB-3 LAYOUT

The layout of the HFIR HB-3 beam tube has a view through the biological shielding and reactor pool at a location just off the fuel assembly's center vertical axis. The centerline defined by the axis of this tube will provide the best location for optical components (apertures, filters, imaging plane, etc.), and it will define the nominal trajectory of the beam for all estimates of performance. As currently designed, a coarse internal collimator insert provides the initial defining view of the moderated neutron flux. The collimator begins at about 280 cm from the entrance of the beam tube and is 91 cm long. The exit of the collimator is at the entrance of the main shutter cavity. These features, as well as rough boundaries for the instrument layout, are depicted in Figure 3-1.

These layout boundaries would permit an aperture-to-imaging plane distance of up to 350 cm, assuming that the final defining aperture could be located within the shutter cavity. This would provide a field of view on the order of 8 cm wide based on the location of the aperture relative to the source and the possible imaging plane distance. This was the starting geometry chosen to analyze the proposed concept capability and to provide further optimization for the proposed science cases.

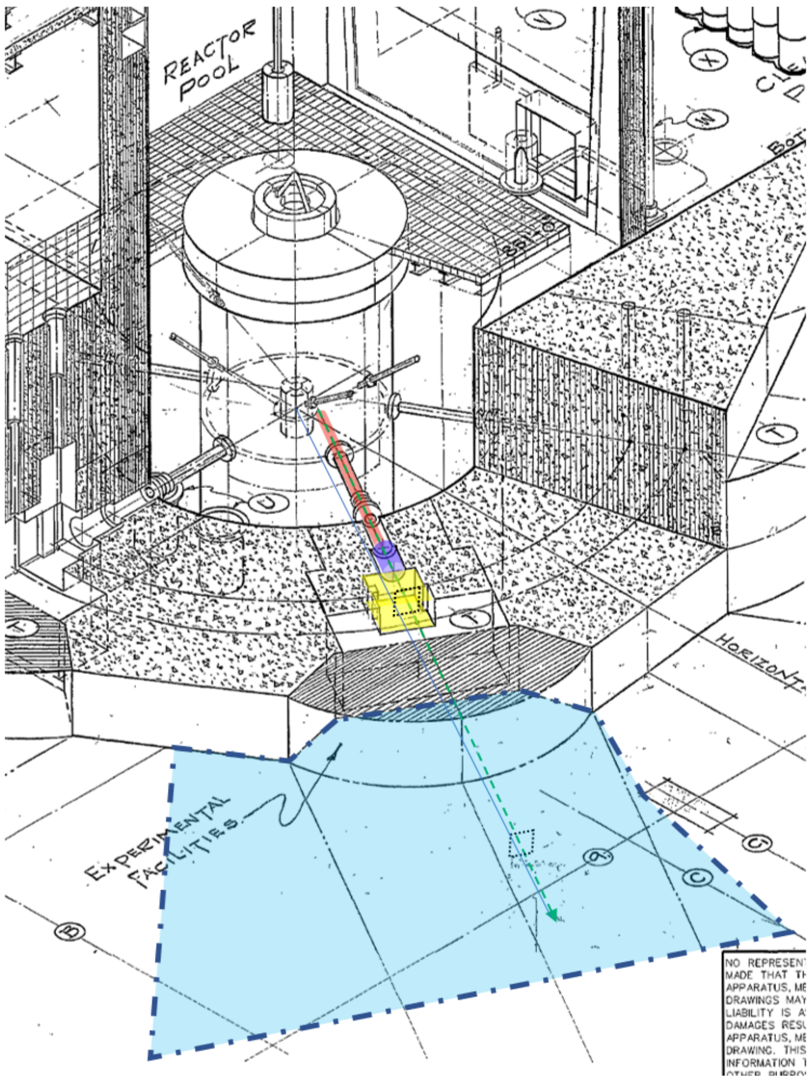

Figure 3-1. Rough HFIR HB-3 beam tube layout defining key locations and relative position of the beam tube (orange), coarse collimator (purple), shutter cavity (yellow), proposed experiment floor boundaries (light blue), nominal beam trajectory (green arrow), and imaging plane (black dashed square).

3.2 NEUTRON AND GAMMA FLUX CHARACTERISTICS AT HB-3 ENTRY

Neutron and gamma transport analyses were performed using MCNP to assess the current neutron source capability available for fast neutron radiography on HB-3, to assess the gamma background, and to obtain a neutron source that could be used for a conceptual collimator design. Figure 3-2 and Figure 3-3 show horizontal and vertical sections through the MCNP HFIR model (Chandler and Betzler 2015), and Figure 3-4 shows the model overlayed onto a model of the HFIR building.

The neutron and prompt gamma fluxes and spectra were computed at the beam tube entrance of HB-3, as shown in Figure 3-2. Figure 3-5 shows the total forward neutron flux of 3.97×10^{14} n cm^{-2} s^{-1} and its spectrum at the beam tube entry, and Figure 3-6 shows the total forward prompt gamma flux of 4.85×10^{14} phot. cm^{-2} s^{-1} and its spectrum. The neutron flux resembles the usual thermal neutron reactor spectrum in the reflector with the Maxwellian peak in the thermal region and a 1/E spectrum dependence in the fast region. The majority of the gamma rays have energies in the 1×10^{-2} to 1 MeV range, with the 1–10 MeV range small, but likely not negligible. The impact of the gamma irradiation of the facility components requires further evaluation and must be accounted for in the facility design.

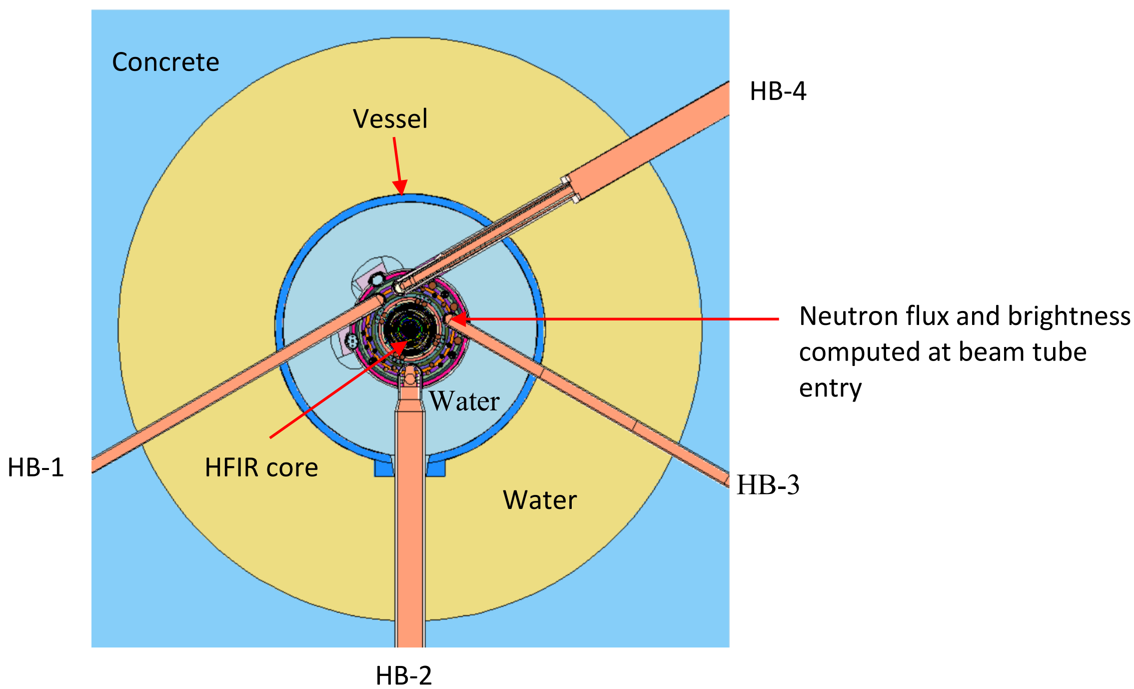

Figure 3-2. Top view of HFIR MCNP model.

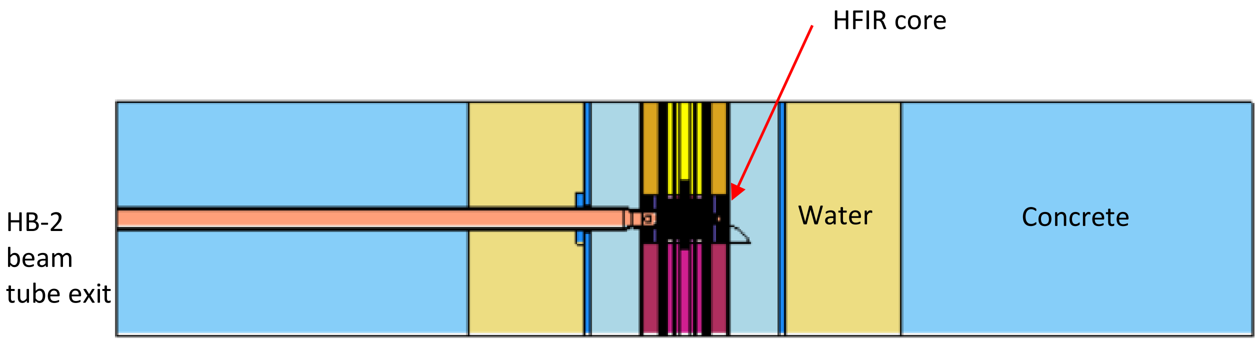

Figure 3-3. Side view of HFIR MCNP model through HB-2.

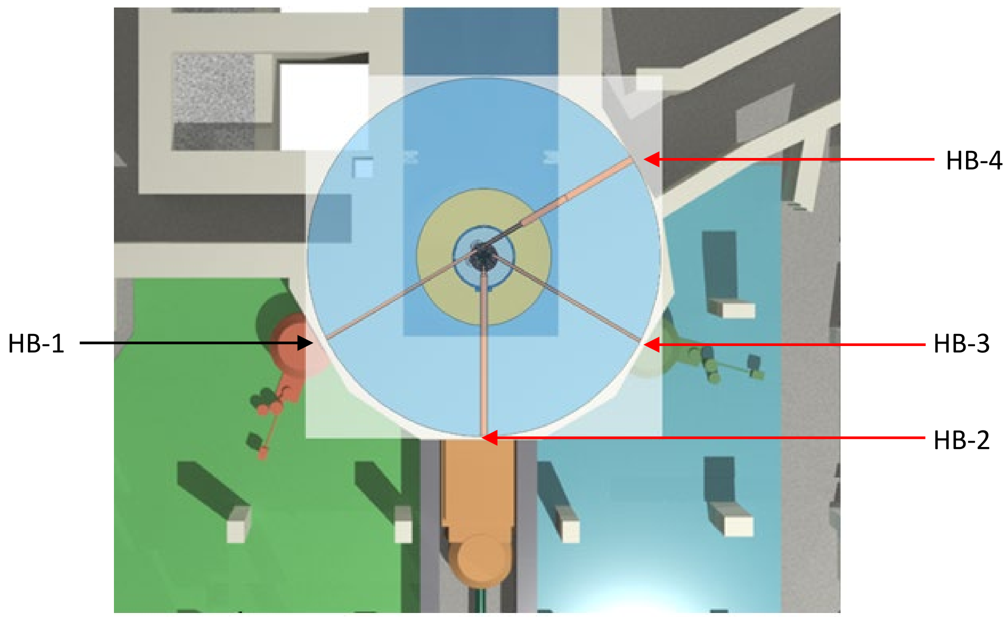

Figure 3-4. MCNP model overlayed onto HFIR building model.

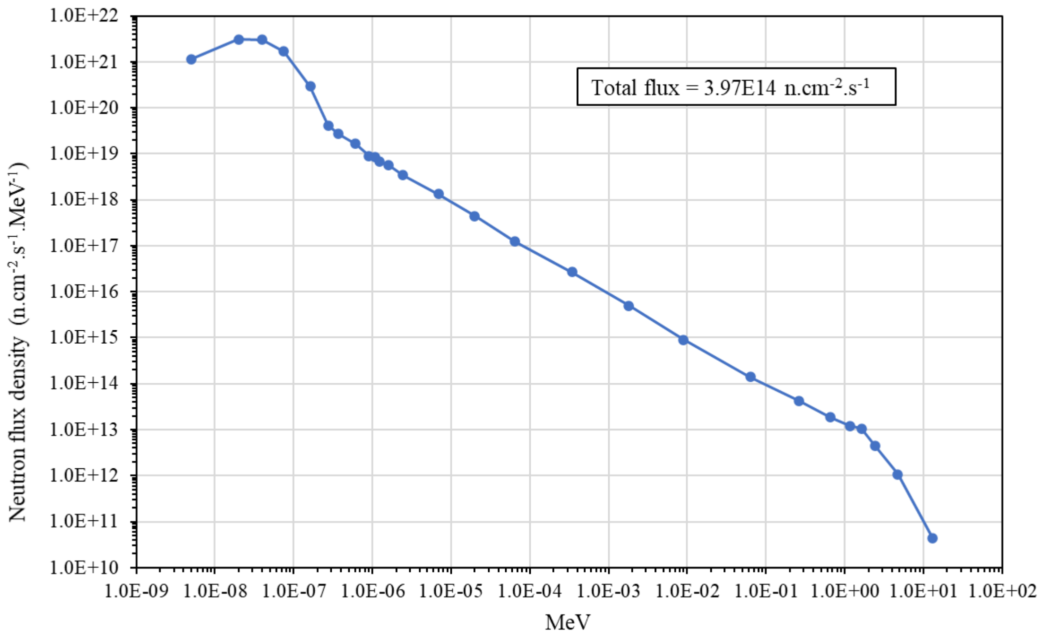

Figure 3-5. Forward neutron flux at HB-3 beam tube entry.

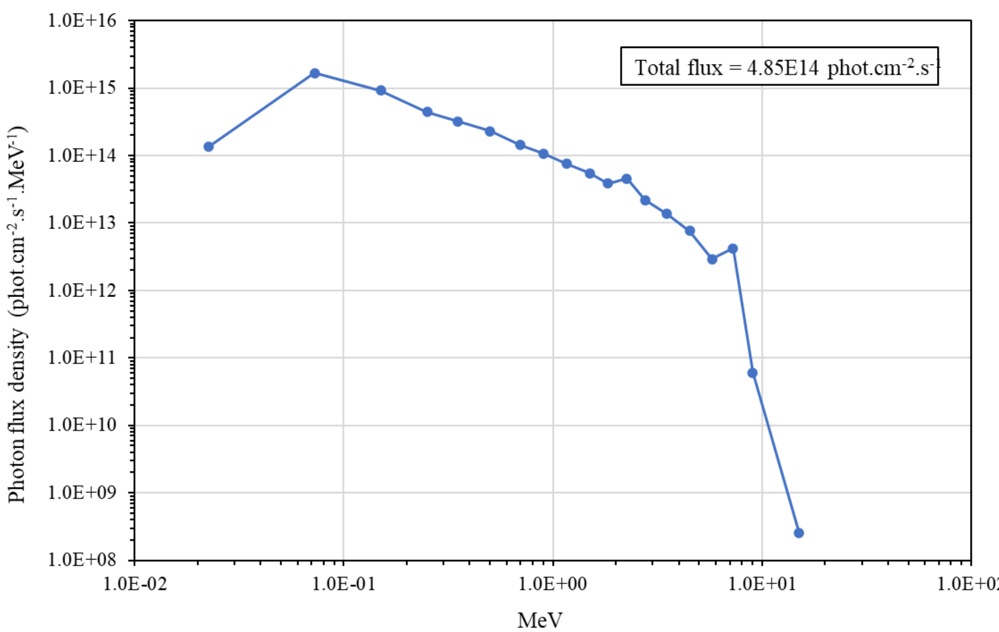

Figure 3-6. Forward gamma flux at HB-3 beam tube entry.

3.3 NEUTRON BRIGHTNESS FOR CONCEPTUAL COLLIMATOR DESIGN

Epithermal neutron radiography occurs roughly in the 0.3 eV to 10 keV region, and fast neutron radiography occurs in the 10 keV to 20 MeV region (Rant and Balaskó 2013). To develop the conceptual design for an epithermal radiographic system on HB-3, an epithermal neutron source over the energy range of 0.1 eV to 10 keV was calculated at the beam tube entry using MCNP. The average spatial neutron brightness (also known as the *angular neutron flux*) into an opening angle of about 1° was computed at the beam tube entry. The opening angle was obtained by considering the beam tube diameter (5.08 cm) and the distance to the beam tube exit at the biological shield (approximately 682 cm from the entrance), as shown in Figure 3-7. The total brightness was calculated as 2.3×10^{13} n cm^{-2} sr^{-1} s^{-1}, 0.5° about the beam axis. The surface averaged spectral brightness over the beam tube entry is shown in Figure 3-8.

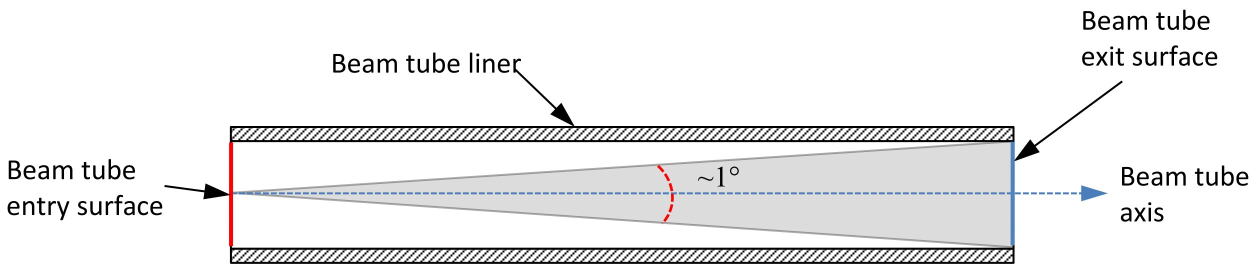

Figure 3-7. HB-3 neutron brightness calculation detail.

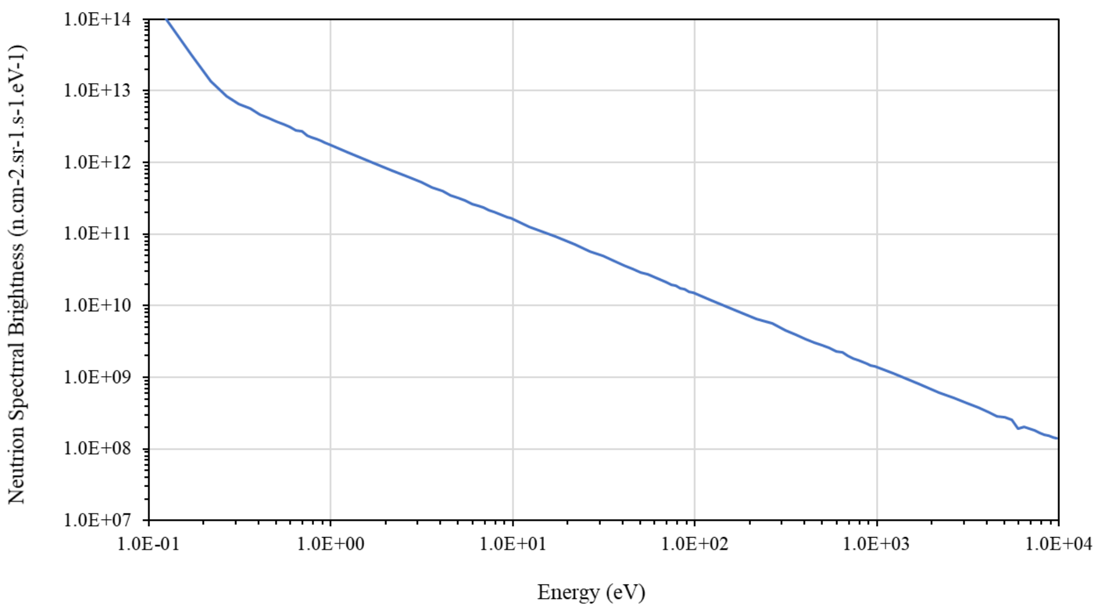

Figure 3-8. HB-3 neutron brightness spectrum determined using MCNP and defined angular trajectory range.

3.3.1 Conceptual Design

Ray tracing and Monte Carlo methods were used to develop the epithermal and fast neutron radiography concept. McStas (Willendrup and Lefmann 2021) is a common ray-tracing software used to develop thermal and cold neutron scattering instrumentation and can be adapted to work with epithermal and higher energies. However, any particle conversion that occurs as a result of absorption of the neutrons is not accounted for, only the attenuation effects in the neutron channel are included. In this case, MCNP can be used to understand any contribution that the aperture and filter geometries will have on the background in the detector.

The McStas ray-tracing capability is an efficient way to gain information about performance attributes because the neutron source is an input surface boundary condition derived from a full 3D Monte Carlo calculation. In this work, the neutron source is strictly an emission area with a specified spectral brightness. McStas minimizes the computational burden even more by only emitting rays that will interact with the *next* optical element in the chain. The result is a fully corrected value for the intensity and statistically relevant values in a short computational time. Detailed development and performance of this design are addressed in Section 3.4.

As noted above, modeling began with a simple view of the fuel assembly through the length of the beam tube and coarse collimator. McStas uses a simple circular area source with a defined brightness spectrum extracted from the HB-3 beam entrance in the HFIR MCNP model. Because the amount of the tally flux that makes it through the tube and collimator is limited in trajectory, the spectral brightness was determined based on the tally flux and the relevant angular emittance range shown in Figure 3-8. This brightness was then integrated into a new McStas source component to baseline the capability and to further optimize the imaging instrument. The code developed for this analysis can be found in the Git repository created for this project: https://code.ornl.gov/3xf/hb3_epithermal_imaging.git (Frost 2022).

3.4 COLLIMATOR DESIGN

As noted in Section 3.3.1, McStas can be used to evaluate imaging performance across a wide parameter space. In particular, finding a balance between image resolution and imaging exposure time is crucial to ensuring a productive imaging capability. This begins by using the determined brightness spectrum described by Figure 3-8 in a simple source component that begins at the tube's entrance. Using the current tube geometry and the exit collimator geometry will provide a suitable start to the optimization process.

Figure 3-9 shows an illustration of the McStas model. Based on the layout depicted in Figure 3-1, there is about 4 meters of space available in the beam room to accommodate an aperture near the shutter position and the imaging plane location. Therefore, an aperture-to-sample distance, *L*, of no more than 350 cm is assumed. In addition, the prototypical sample to be imaged in the instrument is a nuclear fuel irradiation capsule with an assembly diameter of about 12.5 mm, so the imaging plane is set to no less than 15 mm downstream from the sample position center, and 20 mm is used for a low-end performance estimate.

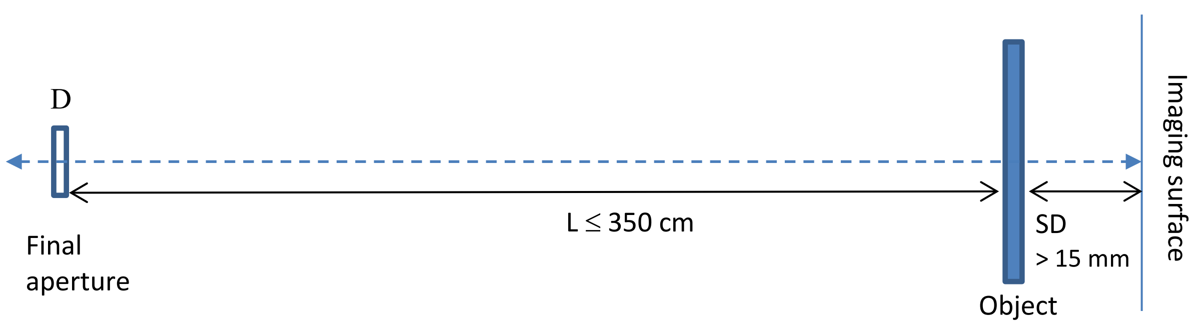

Figure 3-9. A schematic describing the imaging layout parameters: aperture diameter (*D*), aperture to sample distance (*L*), and sample to imaging surface distance (*SD*).

For the initial simulations, perfect aperture performance (perfect opacity) and an imaging surface with 100% efficiency are assumed. The objective is to gain some understanding of the actual neutron spectral flux and image resolution and then to match the imaging plane converter after the beam has been optimized. The code used for this optimization can be found in the previously referenced Git repository (Frost 2022). The simulation begins with the flux density at the center of the field of view. For optimization purposes, this will be a 20×20 mm square centered on the beam axis. The figures of merit for optimization are a maximized flux between 0.2 and 1.0 eV and a spatial resolution no less than 100 microns (0.010 cm).

A sensitivity study was performed over a reasonable range of L, D and SD to analyze system performance under various imaging conditions. As seen in Figure 3-10 and Figure 3-11, flux is kept above 10^9 while still maintaining greater than 0.01 cm resolution and 10 cm field of view using $L \leq 350$ cm, 2 cm $\leq D \leq 3$ cm, and $SD \leq 2$ cm. This configuration will suit the fuel rod assembly geometry and resolution requirements. Further details in the filter and radiological design and should use $L = 350$ cm and 250 cm with $D = 3$ cm to represent the highest total beam intensity on the sample closest to the areas accessed by personnel. Any design changes that impact the beam flux under these conditions would scale linearly across the other D and L configurations.

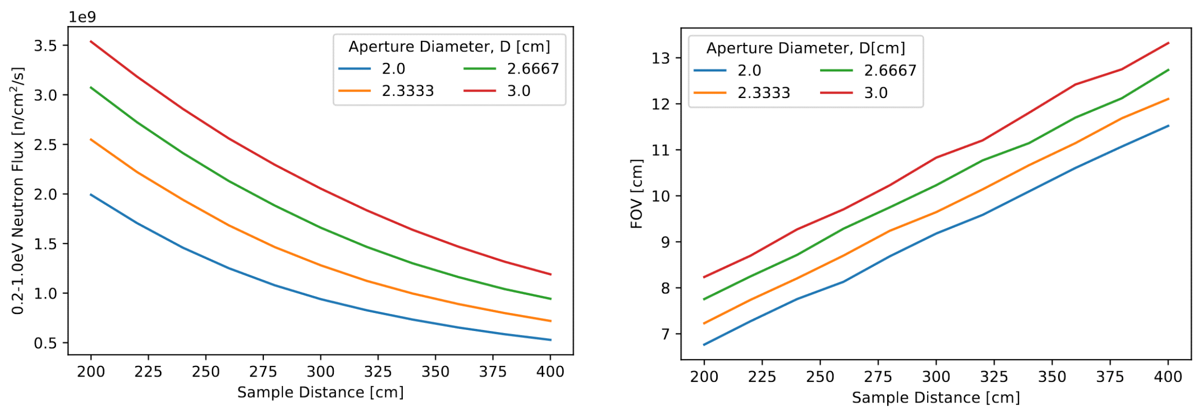

Figure 3-10. Scans showing the neutron flux vs. distance (left) and change in the field of view for varied aperture sizes.

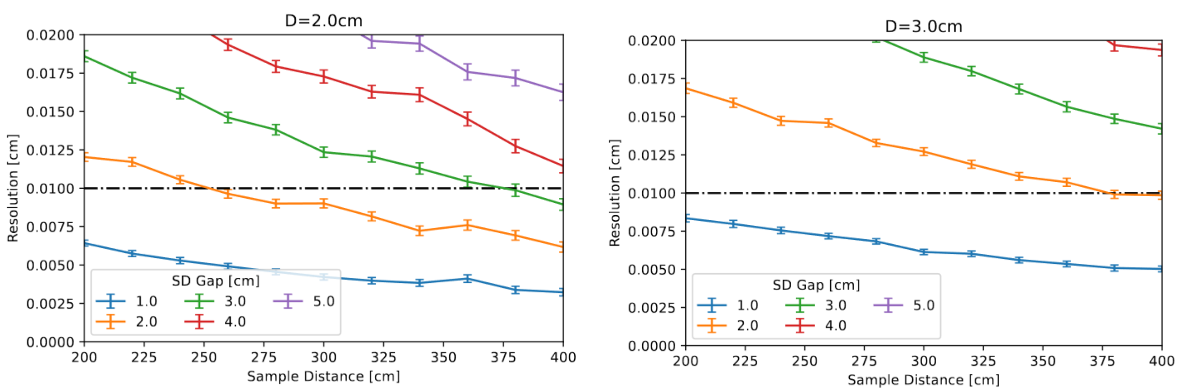

Figure 3-11. Scans showing the change in resolution vs. distance from the aperture for two different aperture sizes and gaps between the detector plane and the sample position.

3.4.1 Fuel Pellet Test Sample

To analyze the performance beyond what is achieved using the beam analysis described above, a test pellet component was developed for McStas to provide some insight into the resolving power of the instrument under representative conditions. The test pellet is a faceted volume with small voids and a simulated crack inside. A wire-mesh view of the test pellet can be seen in Figure 3-12. The component was developed with void diameters ranging from 20–200 µm and a crack path with a cross section diameter of 100 µm. The material simulated for this radiographic test is 20% enriched UO_2 with a density of 10.97 g/cm^3.

Figure 3-12 shows a wire-frame representation of the test model produced using computer-aided design (CAD) and a plot of a log-adjusted, normalized radiographic image of that pellet in the simulated instrument. As the figure shows, even with 0.01 cm binning on the image plane, many of these fine features are visible. These can be refined further with tomographic imaging processes and a higher resolution imaging plane. Further analysis is needed to analyze the actual imaging apparatus' sensitivity to backgrounds and dynamic ranging capability to determine whether this level of sensitivity is achievable in actual circumstances. Nonetheless, this analysis shows that the beam can be prepared to meet the imaging requirements.

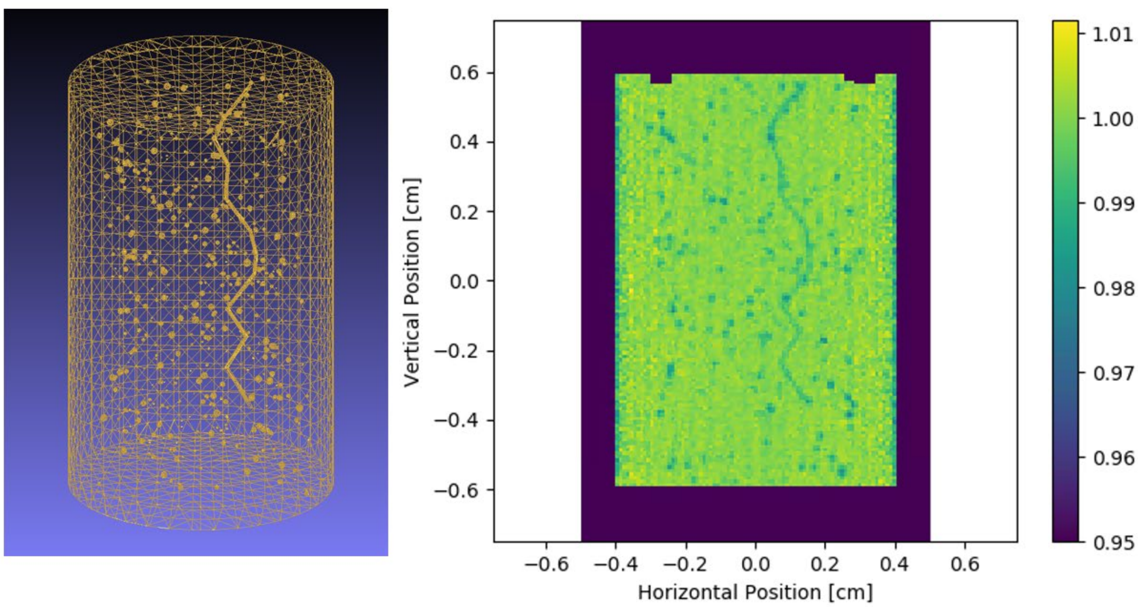

Figure 3-12. A perspective view describing the fuel pellet test geometry as built in CAD software (left) and a corrected plot of the same geometry in the epithermal beam simulation (right).

3.5 IRRADIATED SAMPLE SOURCE STRENGTH

A primary function of the proposed HB-3 epithermal and fast neutron imaging station would require radiography or tomography of encapsulated nuclear fuel samples or isotope production targets irradiated in the vertical experiment facilities (VXF) of the HFIR beryllium reflector. These targets are highly radioactive following irradiation with a significant gamma source from fission and activation products. These high gamma dose rates require substantial shielding for transportation, and preclude the use of direct photosensitive imaging techniques such as x-ray radiography because the sample would saturate the imaging detector. To estimate the source strength characteristics of a hypothetical target, coupled neutron transport and depletion calculations were performed for a UO_2 and NpO_2 target irradiated for one 26-day HFIR cycle using the High Flux Isotope Reactor Controller (HFIRCON) modeling code (Daily, Mosher et al. 2020).

Geometric representations of two irradiation targets were created as an MCNP input file and placed within the inner small VXF-15 facility of a HFIR MCNP model (Xoubi and Primm III 2005). The targets consisted of 6.38 mm diameter pellets encapsulated in grade 9 Ti cladding with an outer diameter of 8.0 mm. Pellets were 6.45 mm in length, with 80 pellets per target, extending almost the full length of the Be reflector. The pellets were composed of high purity NpO_2 ($\rho = 10.07$ g/cm^3) and UO_2 ($\rho = 10.96$ g/cm^3, 3 weight percent enrichment ^{235}U), surrounded by HFIR light-water coolant (Figure 3-13). Although other irradiation target geometries are expected—particularly light-water reactor fuel with pellets 8–11 mm in diameter and cladding 12 mm in diameter—the as-modeled geometry provides a suitable estimate for determining source strength and shielding requirements.

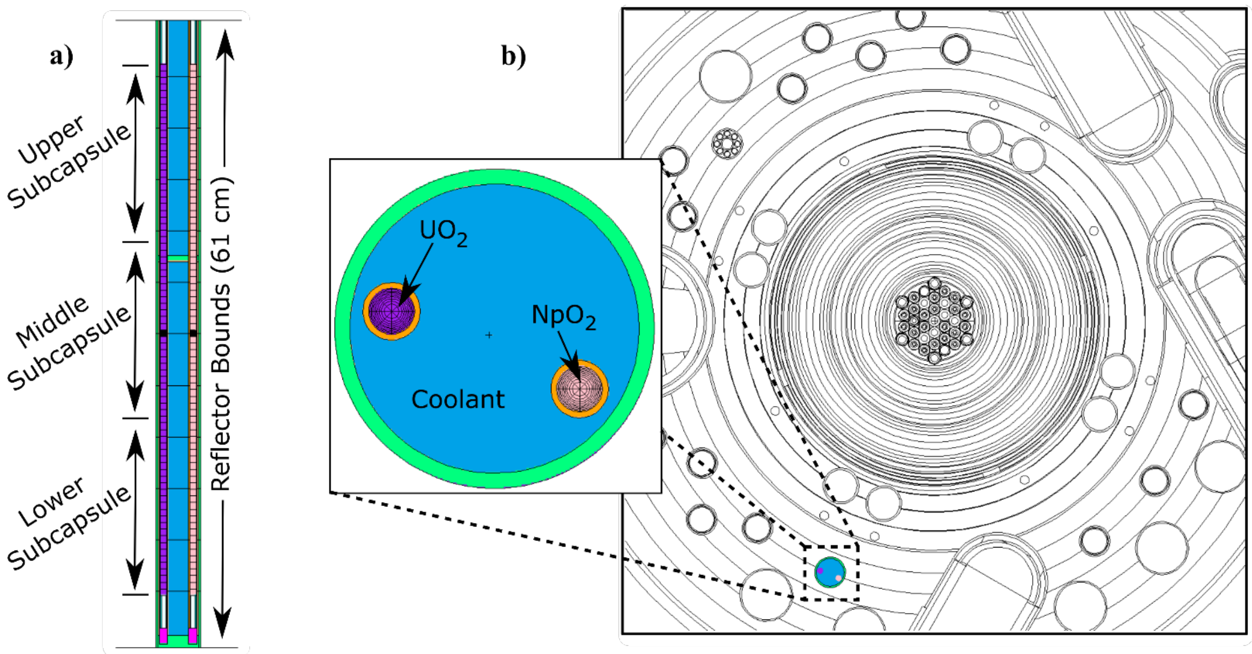

Figure 3-13. Visualizations of MCNP target geometry for (a) elevation view and (b) reactor midplane cross-sectional view of UO_2 (purple) and NpO_2 (pink) targets in HFIR VXF-15 position.

MCNP geometry and material definitions were ported into the HFIRCON code for analysis of one 26-day HFIR cycle. HFIRCON is an ORNL-developed software comprised of several nuclear modeling codes for performing coupled radiation transport and depletion calculations, including the LAVA Model Interrogator (LAVAMINT) code for stochastic calculation of cell volumes, the Automated Variance Reduction Generator (ADVANTG) code used for variance reduction via source biasing and weight window generation (Mosher, Bevill et al. 2013), the ORNL-Transformative Neutronics/MCNP5 (ORNL-TN/MCNP5) code for improved efficiency radiation transport modeling (Mosher and Wilson), the Oak Ridge Isotope Generation (ORIGEN) code for isotopic depletion (Gauld, Radulescu et al. 2011), and various C and python modules for data transfer between programs.

Total isotopic inventories were analyzed following HFIRCON modeling and were found to be well over 15 kCi for each target immediately following irradiation, remaining above 1 kCi for 120 days for UO_2 and 40 days for NpO_2, respectively. The majority of this activity is from gamma, alpha, and beta decay, with little-to-no neutron emission. However, these total activities represent a full length (~61 cm) irradiation target spanning the Be reflector. While transporting and imaging targets of this length would be theoretically feasible, subdividing the targets into three equal lengths was determined to be much more manageable. Radionuclide inventories calculated by HFIRCON were therefore subdivided into ~17 cm segments representing 26–27 pellets per subcapsule. The energy-dependent gamma spectra were calculated for the middle UO_2 and NpO_2 subcapsules for 5, 30, and 365 days following irradiation (Figure 3-14, Figure 3-15). This middle subcapsule represents the maximum gamma intensity for one cycle of irradiation.

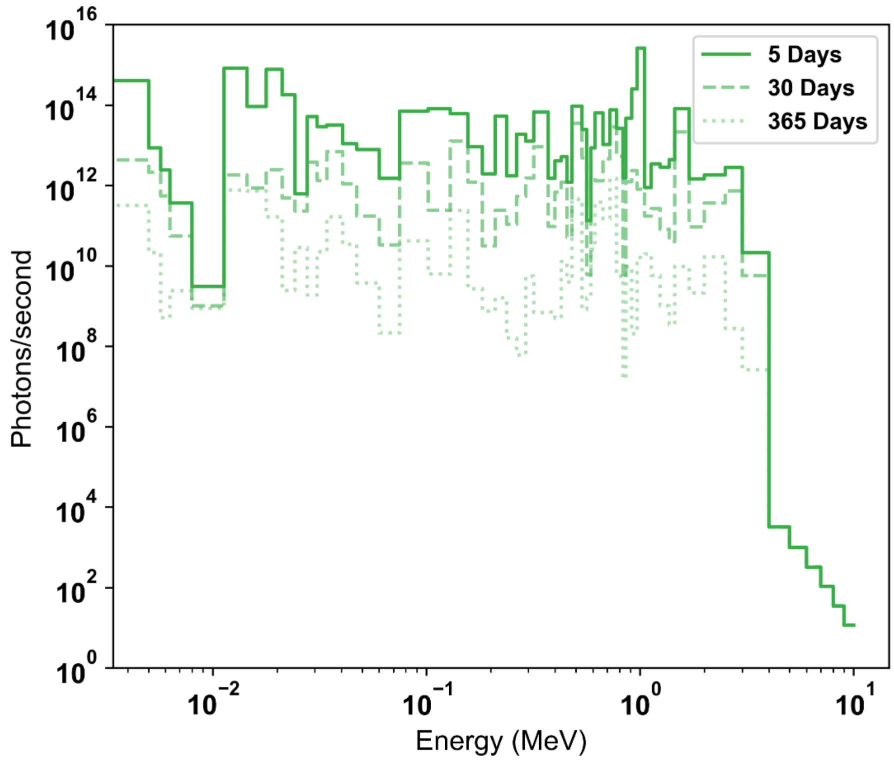

Figure 3-14. Photon spectra for middle subcapsule of 26 NpO_2 pellets irradiated for one HFIR cycle in the VXF-15 position.

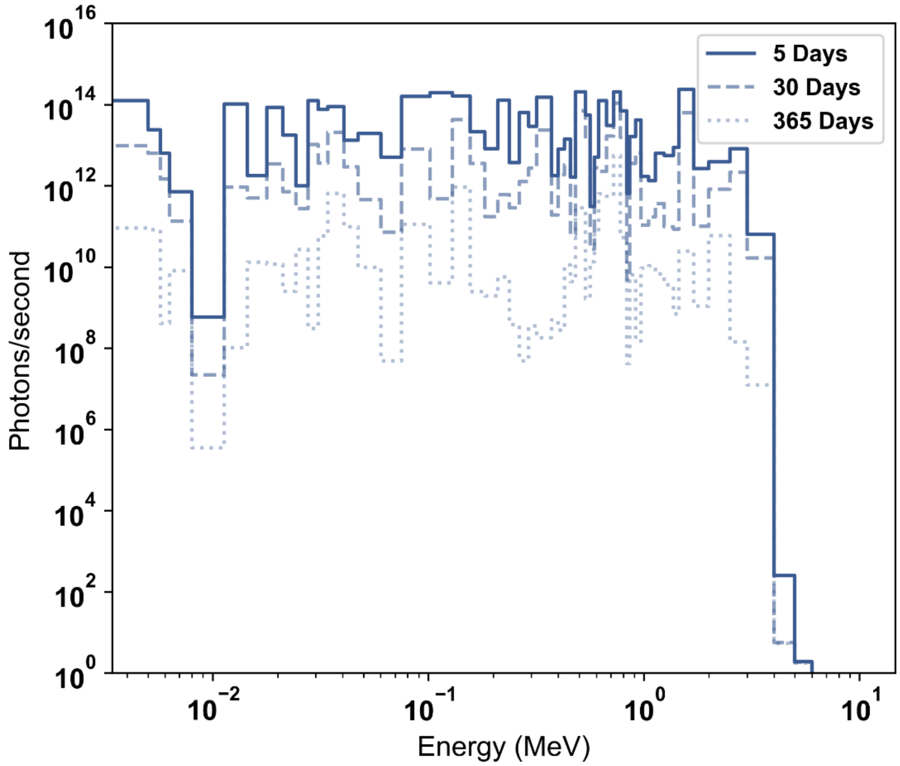

Figure 3-15. Photon spectra for middle subcapsule of 26 UO_2 pellets irradiated for one HFIR cycle in the VXF-15 position.

As Figure 3-14 and Figure 3-15 illustrate, this intense gamma source would be problematic for imaging with techniques susceptible to photon interaction, or easily damaged from prolonged exposure such as CCD cameras. To determine the extent of this issue, the unshielded dose rates (Si equivalent) were calculated from the gamma spectra for NpO_2 and UO_2 targets at 1 m and are shown in Figure 3-16. As this figure shows, dose rates remain quite high (> 100 Gy) for 40–60 days after irradiation. However, other high radioactivity facilities such as NRAD have demonstrated proficiencies in radiographing samples with similar or greater source strengths (Craft, Wachs et al. 2015) and should be achievable in the proposed HFIR facility.

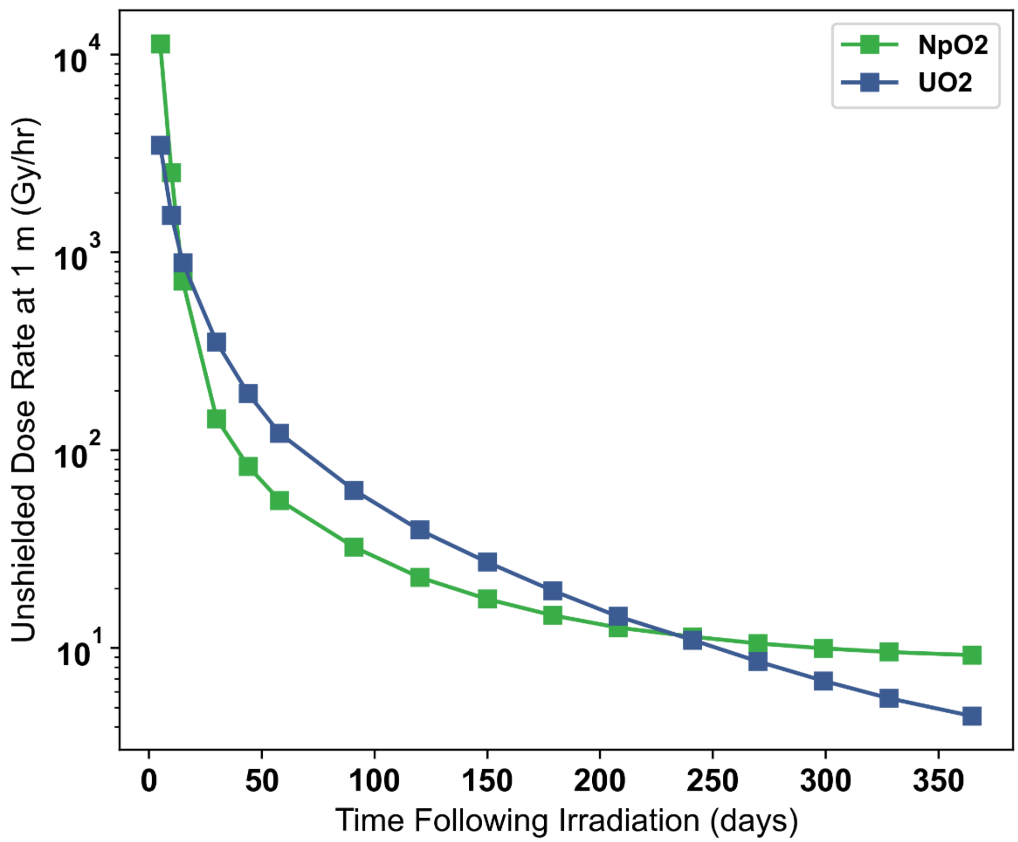

Figure 3-16. Unshielded dose rate (Si equivalent) at 1 m following one cycle of irradiation.

3.6 FACILITY SHIELDING AND TRANSPORTATION LOGISTICS

Performing neutron radiography on an irradiated target requires a logistical plan for the transportation of the target from the small VXF position in the reactor to the experiment area in the HB-3 HFIR beam room. To safely transport the irradiated target, it will need to be enclosed within a shielded transport cask. It is preferrable to use an existing HFIR transport cask design to avoid the costs associated with designing, fabricating, and qualifying a new model. It is also highly desirable to avoid transporting the target outside the HFIR building, which would require additional transportation approvals and would increase the cost of transporting each target.

An assessment of several existing transport casks used by HFIR showed that the Sugarman S-10-13 cask model is the best existing option for the transport of irradiated targets. The Sugarman design is the lightest existing cask, providing enough internal space to load a typical small VXF target. The Sugarman cask is approximately 50 cm in length and 50 cm in diameter, with an interior compartment 25 cm in length and 18 cm in diameter for containing radioactive materials. The dimensions of this interior compartment are compatible with the length of the target subsections described in Section 3.5. The target can be loaded into the cask in the reactor bay and lowered into the first floor experiment room through an existing access hatch. From there, the cask can be moved to the elevator and transported to the ground floor. The Sugarman cask design weighs 2,400 lb and is light enough to be loaded onto the existing HFIR elevator, which has a capacity of 10,000 lb. Once the cask is on the ground floor, it can be transported to the neutron radiography experiment area in the HB-3 beam room using a manually operated, transportable hoist.

Dose rates for radioactive shipments are generally limited to 200 mrem/hr at the shipping container's surface under 49 CFR 173.441. To assess whether the Sugarman S-10-13 cask was sufficient for shielding the prototypic NpO_2 and UO_2 targets, a simple 1D calculation for dose rate at the cask surface was performed assuming 6.125 inches of lead and 0.375 inches of stainless steel. A photon buildup factor was not included. Results of this calculation for various time intervals following irradiation are shown below in Figure 3-17. For one cycle of irradiation, a target would be suitable for shipment using the large Sugarman cask after approximately 53 days for a NpO_2 target and after 79 days of decay for a UO_2 target.

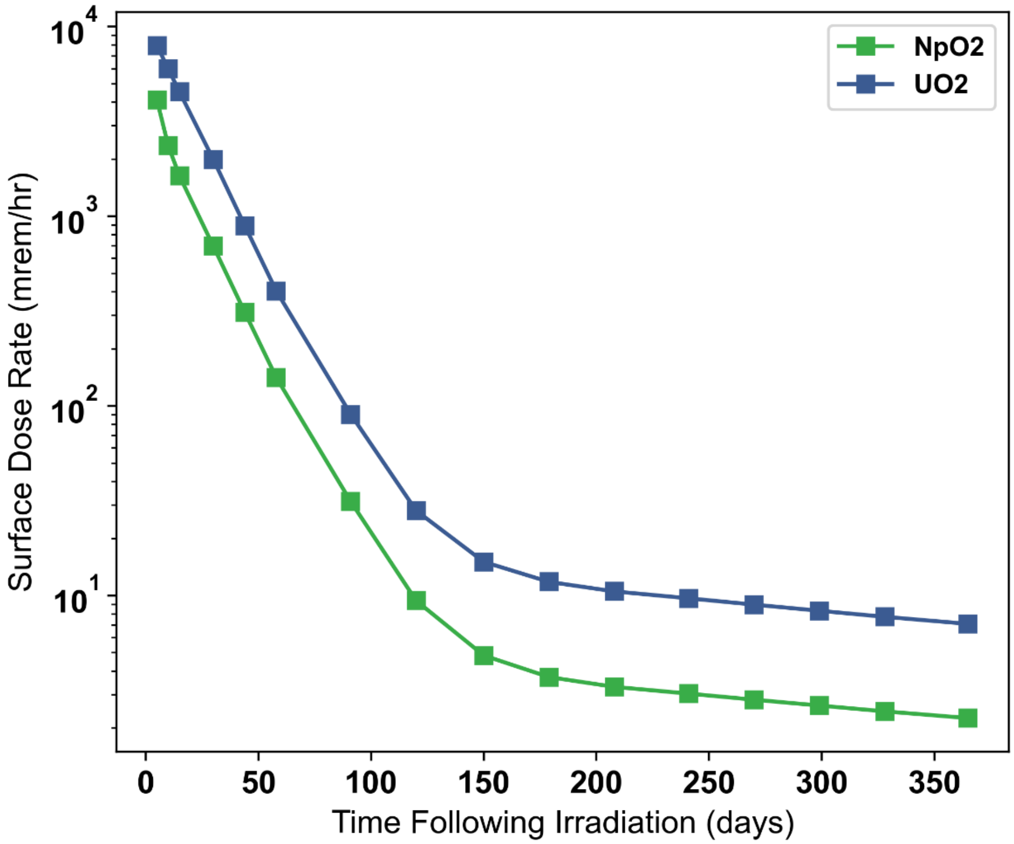

Figure 3-17. Dose rate on surface of large Sugarman shipping cask following different decay time intervals following one cycle of irradiation.

Once the cask has been transported to the fast and epithermal imaging station, additional shielding will be required in a modular hot cell to position the sample in the neutron beam. The hot cell would be positioned in the beamline, with entrance and exit openings to allow the beam to traverse the facility. Thin windows of Al would remain in place to maintain a hermetic environment inside the hot cell, and additional Pb shieling could be removed when performing imaging. Figure 3-18 presents a conceptual model for this facility to scale with approximate dimensions for the beam tube, collimator, shutter, and beam stop locations.

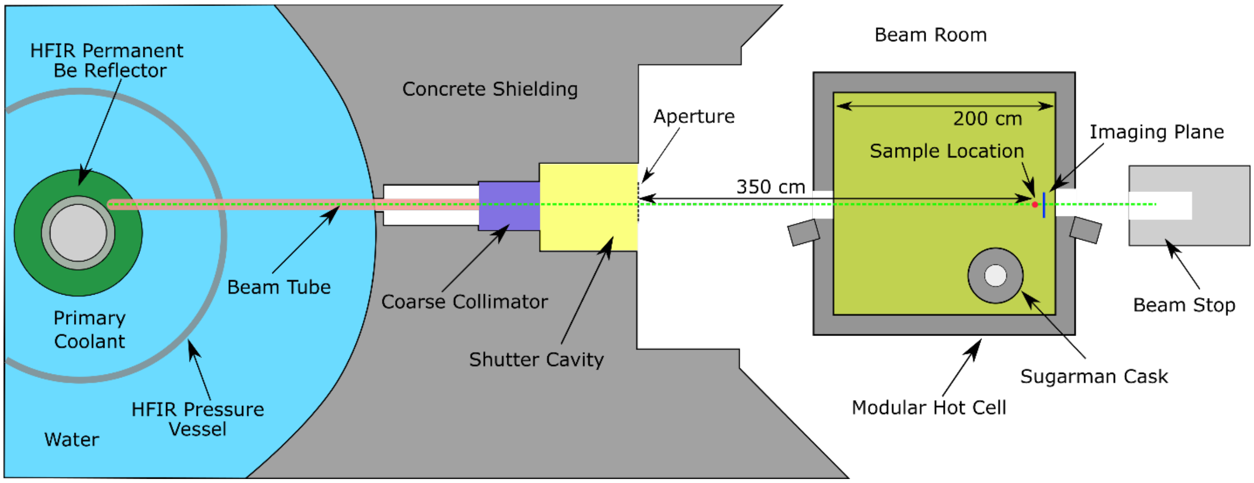

Figure 3-18. Plan view of proposed hot cell enclosure for epithermal beamline.

4. CONCEPTUAL PROPOSAL

Using the design suggestions described in Section 3.4, the imaging plane would be located approximately 350 cm from the final beam aperture. A modular hot cell with a 2×2 m internal footprint would be sufficient for housing the transportation cask, rotational and translational sample stage, imaging equipment, and support equipment. A hot cell wall composed of Pb with thickness equivalent to that of the transportation cask (~15.5 cm) was assumed for this conceptual design. The imaging equipment could be located outside of the hot cell facility to avoid transferring imaging plates into and out of containment, but the imaging resolution would be degraded by the exit window. The hot cell would be equipped with a sufficiently large entrance door to accept the transportation cask, a small winch for lifting the lid of the cask, and manipulator arms for moving the sample into place for imaging. The height of the beam tube is approximately 107 cm above floor level in the beam room, providing sufficient space to store the Sugarman transportation cask below the beam, as shown in Figure 4-1.

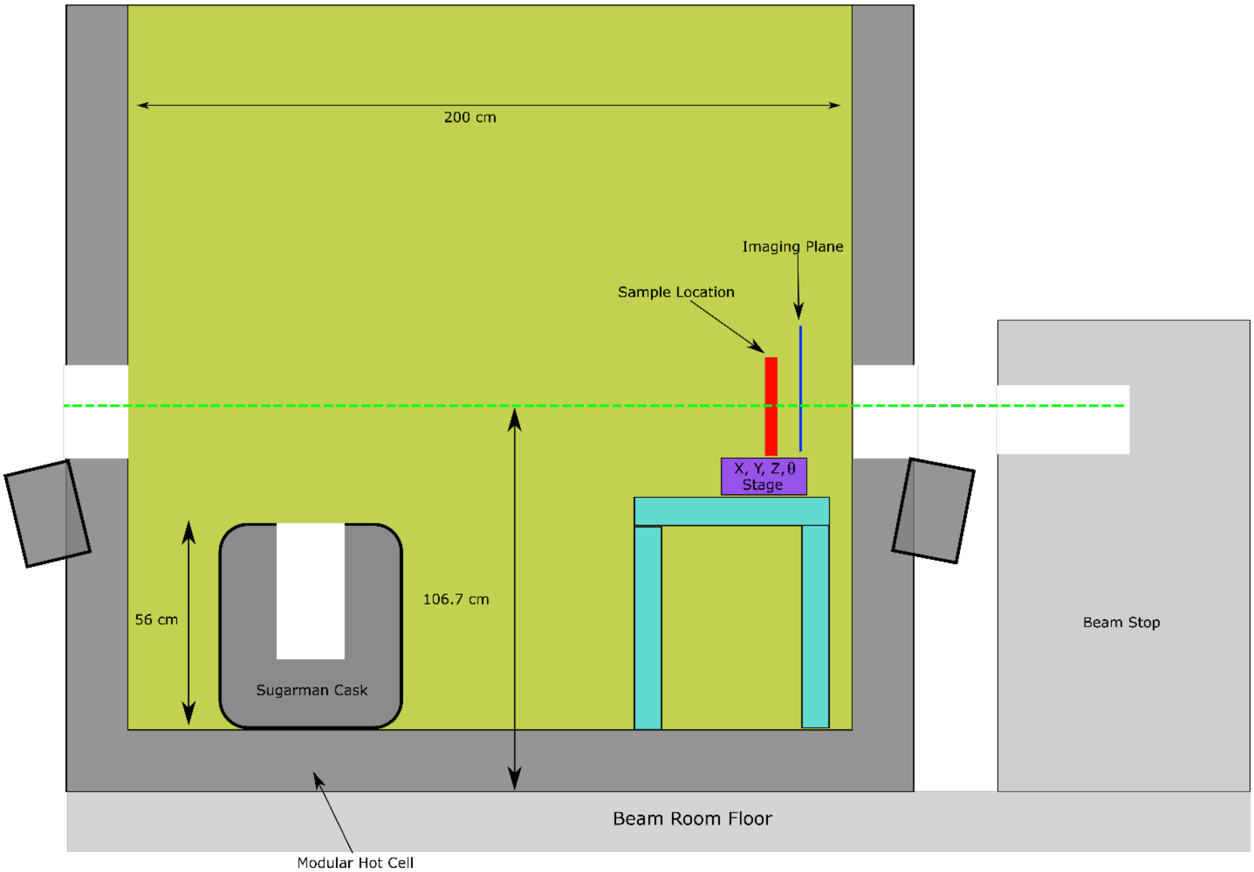

Figure 4-1. Elevation view of hot cell facility with imaging equipment and transportation cask.

4.1 IMAGING AND DETECTION SYSTEM

Because of the intense unshielded gamma activity of the proposed sample materials, the only viable imaging technique is likely an indirect foil film transfer method using Dy, In, or both, as used at INL's NRAD and at NEURAP (PSI-SINQ). These techniques should provide resolution sufficient for imaging small voids and cracks (~100 µm) in the fuel pellets and could be used for coarse tomography as done by Vontobel at the NEURAP facility (Vontobel, Tamaki et al. 2006). Although this technique is most appropriate for highly radioactive samples, the facility should be designed with the capability to use CCD or microchannel plate detectors for other nonradioactive specimens. This type of imaging system could be located inside of or directly behind the modular hot cell and would add a rapid, high-resolution alternative detection system for the facility when other low activity samples are being imaged.

4.2 ADDITIONAL REQUIREMENTS

Minimal additional infrastructure requirements would be necessary for the development of this facility. The existing chilled water, process air, inert gas cylinders, electrical power (possibly 480 V) and connection to the HFIR hot off-gas system would be sufficient. Further analysis into floor loading from the weight of the modular hot cell would be necessary but should be comparable to other large instruments installed in the beam room. Radiography of irradiated fuel specimens is estimated to take 1–2 days and would require that the accountable material be left unattended overnight. Therefore, the hot cell facility requires a nuclear materials control and accountability (NMC&A) storage area designation.

4.3 ALTERNATIVE OPTIONS CONSIDERED

The working group considered several design modifications, including tilting the beam port within the reflector. However, it was decided that no modification with respect to viewing the fuel is needed and that the existing epithermal and fast neutron flux in HB-3 was sufficient. Dynamic testing on irradiated fuel was also considered, including cladding burst measurements, load frame testing, furnace environments, and hydride reorientation studies. However, these tests were deemed to be overly complicated for the limited space available in the modular hot cell and would increase the likelihood of dispersing contamination in the facility.

4.4 ASSET BENEFITS

Hydride accumulation in cladding of fuel rods in light-water reactors is a limiting factor for longer fuel irradiations and more efficient operations in nuclear power plants. While the density and spatial distribution of hydrides is typically analyzed through destructive sectioning of small segments of cladding, neutron radiography offers the potential to examine much larger sections of fuel rods nondestructively (Groeschel, Schleuniger et al. 1999). The high penetrability of neutrons in uranium and the high scattering cross section of hydrogen makes neutron radiography or tomography an effective technique for examining the presence of hydrogen. X-ray imaging of such targets would prove difficult or impossible, because the high-Z material of transuranics are opaque to x-rays, hydrogen is nearly transparent, and the high gamma field from the sample under investigation would saturate an x-ray detector or film. Epithermal or fast radiography is often the preferred approach for this examination because isotope cross sections are comparable in this energy range.

4.5 COST AND SCHEDULE ESTIMATES

Although detailed mechanical designs and further neutron transport analysis are required, an epithermal/fast neutron facility as described in this report is estimated to cost $40–60 million. Installation would require some reconfiguring or replacement of components in the beam tube and shutter, which could increase this estimate. Design, procurement, assembly, and commissioning of the facility are expected to require two years of effort.

4.6 FUTURE ANALYSIS

This report provides a conceptual design for an epithermal and fast neutron imaging facility. Although many of the technical details were analyzed and demonstrate that this facility is feasible and competitive with other user facility concepts, additional analyses will be required. Areas of further investigation should include the following:

- Optimization of the beam stop for fast neutrons
- Detailed modeling of shielding and floor loading of the modular hot cell
- Background generated by an epithermal/fast beam facility in other nearby equipment
- Analysis of appropriate filtering materials, possibly with transmission measurements at other HFIR or SNS facilities

5. CONCLUSIONS

ORNL's HFIR SENSe initiative offers a unique opportunity to explore new scientific capabilities for HFIR and the laboratory. As part of this initiative, a working group of scientific staff members developed a conceptual design for an epithermal and fast radiography instrument on the existing HB-3 HFIR beamline. Epithermal and fast neutron radiography provides an examination technique that is complementary to x-ray and thermal neutron imaging that would be particularly efficient for use in studies of mixtures of high-z and low-z materials such as nuclear fuels, isotope production experiments, and spallation neutron targets. This instrument would have immediate benefits for future and existing programs, including the Advanced Fuels Campaign, the DOE Isotopes program, and other DOE Office of Science missions. This document summarizes findings and recommendations from this working group, demonstrates that such an instrument is feasible with the current reactor configuration, and is competitive with similar facilities around the world.

6. REFERENCES

Adib, M., N. Habib, I. I. Bashter, H. N. Morcos, M. S. El-Mesiry and M. S. Mansy (2015). "Characteristics of Poly- and Mono-Crystalline BeO and SiO_2 as Thermal and Cold Neutron Filters." *Nuclear Instruments & Methods in Physics Research*. Section B, Beam Interactions with Materials and Atoms **358**: 98–104.

Adib, M., K. Naguib, A. Ashry and M. Fathalla (2002). "On the Use of Lead as a Neutron Filter." *Annals of Nuclear Energy* **29**(9): 1119–1130.

Aizawa, O., T. Matsumoto and S. Watanabe (1986). "Usefulness of Single-Crystal Bismuth and Silicon for Neutron Radiography Facility." *Journal of Nuclear Science and Technology* **23**(6): 562-564.

Al-Qasir, I. and A. Qteish (2017). "Neutron Filter Efficiency of Beryllium and Magnesium Fluorides." *Journal of Applied Crystallography* **50**(2): 441–450.

Bauer, G. S. (1998). "Operation and Development of the New Spallation Neutron Source SINQ at the Paul Scherrer Institut." *Nuclear Instruments and Methods in Physics Research Section B: Beam Interactions with Materials and Atoms* **139**(1): 65–71.

Bilheux, H., K. Herwig, S. Keener and L. Davis (2015). "Overview of the Conceptual Design of the Future VENUS Neutron Imaging Beam Line at the Spallation Neutron Source." *Physics Procedia* **69**: 55-59.

Birgeneau, R., S. Clark, P. Dai, T. Epps, K. Heeger, D. Hoogerheide, M. Kastner, B. Keimer, D. Louca, P. Lyons, A. MacDonald, S. O'Kelly, B. Olsen, J. Phillips, D. Robertson, A. Rollett, K. Ross, M. Rowe, J. Stevens and B. Wirth (2020). "The Scientific Justification for a US Domestic High-Performance Reactor-Based Research Facility." *Report of the Basic Energy Sciences Advisory Committee, U.S. Department of Energy, Office of Science*.

Bryan, C. D. and D. Chandler (2022). "HFIR Futures - Enhanced Capabilities Series: Volume 1: Introduction to the HFIR Futures – Enhanced Capabilities Series." Oak Ridge National Laboratory, Oak Ridge, TN. ORNL/TM-2022/2691/V1.

Bücherl, T., C. Lierse von Gostomski, H. Breitkreutz, M. Jungwirth and F. M. Wagner (2011). "NECTAR—A fission neutron radiography and tomography facility." *Nuclear Instruments and Methods in Physics Research Section A: Accelerators, Spectrometers, Detectors and Associated Equipment* **651**(1): 86–89.

Bucherl, T. and S. Sollardl (2015). "NECTAR: Radiography and Tomography Station Using Fission Neutrons." *Journal of Large-Scale Research Facilities* **1**: A19.

Chandler, D. and B. R. Betzler (2015). "Modeling and Depletion Simulations for a HFIR Cycle with Representative Target Loading (C-HFIR-2015-013)." Oak Ridge National Laboratory, Oak Ridge, TN.

Craft, A. E., D. M. Wachs, M. A. Okuniewski, D. L. Chichester, W. J. Williams, G. C. Papaioannou and A. T. Smolinski (2015). "Neutron Radiography of Irradiated Nuclear Fuel at Idaho National Laboratory." *Physics Procedia* **69**: 483–490.

Daily, C., S. Mosher, S. D. Wilson and D. Chandler (2020). "HFIRCON Version 1.0.5 User Guide." Oak Ridge National Laboratory, Oak Ridge, TN. ORNL/TM-2020/1742.

Dhiman, I., R. Ziesche, T. Wang, H. Bilheux, L. Santodonato, X. Tong, C. Y. Jiang, I. Manke, W. Treimer, T. Chatterji and N. Kardjilov (2017). "Setup for Polarized Neutron Imaging Using in-situ ^{3}He Cells at the Oak Ridge National Laboratory High Flux Isotope Reactor CG-1D Beamline." *Review of Scientific Instruments* **88**(9): 095103.

Freund, A. K. (1983). "Cross-Sections of Materials Used as Neutron Monochromators and Filters." *Nuclear Instruments and Methods in Physics Research* **213**(2): 495–501.

Frost, M. (2022). "HB3_Epithermal_Imaging (Version 1.0) [Source Code]." Oak Ridge National Laboratory, https://code.ornl.gov/3xf/hb3_epithermal_imaging.git.

Gauld, I. C., G. Radulescu, G. Ilas, B. D. Murphy, M. L. Williams and D. Wiarda (2011). "Isotopic Depletion and Decay Methods and Analysis Capabilities in SCALE." *Nuclear Technology* **174**(2): 169–195.

Giegel, S. H., A. E. Craft, G. C. Papaioannou, A. T. Smolinski and C. L. Pope (2021). "Neutron Beam Characterization at Neutron Radiography (NRAD) Reactor East Beam Following Reactor Modifications." *Quantum Beam Science* **5**(2).

Greenwood, R. C. and R. E. Chrien (1976). "Filtered Reactor Beams for Fast Neutron Capture γ-Ray Experiments." *Nuclear Instruments and Methods* **138**(1): 125–143.

Groeschel, F., P. Schleuniger, A. Hermann, E. Lehmann and L. Wiezel (1999). "Neutron Radiography of Irradiated Fuel Rod Segments at the SINQ: Loading, Transfer and Irradiation Concept." *Nuclear Instruments and Methods in Physics Research Section A: Accelerators, Spectrometers, Detectors and Associated Equipment* **424**(1): 215–220.

Ibrahim, O., Z. Matthew Van, B. Matthew, K. Andrew, H. Joel, K. Praneeth, J. C. Nerine and R. C. Lei (2020). "Characterization of a Reactor-Based Fast Neutron Beam Facility for Fast Neutron Imaging." *Proceedings of SPIE Optical Engineering and Applications*, August 16-21, 2020.

Ikeda, Y. (2009). "J-PARC Status Update." *Nuclear Instruments and Methods in Physics Research Section A: Accelerators, Spectrometers, Detectors and Associated Equipment* **600**(1): 1–4.

Kenji, N., K. Yukinobu, I. Shinichi, A. Jun, A. Kazuya, A. Hiroyuki, E. Hitoshi, F. Masaki, F. Kenichi, G. Wu, H. Masahide, H. Stefanus, H. Takanori, H. Masahiro, H. Takashi, H. Akinori, I. Kazutaka, I. Takashi, I. Toru, I. Yoshihisa, I. Hiroki, K. Tetsuya, K. Ryoichi, K. Takashi, K. Naokatsu, K. Daichi, O.-K. Seiko, K. Takuro, K. Atsushi, K. Ryoji, K. Kenji, K. Katsuhiro, L. Sanghyun, M. Shinichi, M. Takatsugu, M. Kenji, M. Koji, N. Mitsutaka, N. Shoji, N. Akiko, O. Tatsuro, O. Takashi, O. Kazuki, O. Hidetoshi, O. Kenichi, O. Toshiya, S.-F. Asami, S. Kaoru, S. Takenao, S. Kazuhiko, S. Jun-ichi, S. Kentaro, T. Atsushi, T. Shin-ichi, T. Masayasu, T. Yosuke, T. Shuki, T. Naoya, L. Y. Norifumi, Y. Taro, Y. Dai, Y. Tetsuya, Y. Masao and Y. Hideki (2017). "Materials and Life Science Experimental Facility (MLF) at the Japan Proton Accelerator Research Complex II: Neutron Scattering Instruments." *Quantum Beam Science* **1**(3): 9.

Kino, K., M. Furusaka, F. Hiraga, T. Kamiyama, Y. Kiyanagi, K. Furutaka, S. Goko, K. Y. Hara, H. Harada, M. Harada, K. Hirose, T. Kai, A. Kimura, T. Kin, F. Kitatani, M. Koizumi, F. Maekawa, S. Meigo, S. Nakamura, M. Ooi, M. Ohta, M. Oshima, Y. Toh, M. Igashira, T. Katabuchi, M. Mizumoto and J. Hori (2014). "Energy Resolution of Pulsed Neutron Beam Provided by the ANNRI Beamline at the J-PARC/MLF." *Nuclear Instruments and Methods in Physics Research Section A: Accelerators, Spectrometers, Detectors and Associated Equipment* **736**: 66–74.

Lehmann, E., P. Vontobel and M. Estermann (2004). "Study of Material Changes of SINQ Target Rods after Long-Term Exposure by Neutron Radiography Methods." *Applied Radiation and Isotopes* **61**(4): 603–607.

Lehmann, E. H., P. Vontobel, G. Frei, G. Kuehne and A. Kaestner (2011). "How to Organize a Neutron Imaging User Lab? 13 Years of Experience at PSI, CH." *Nuclear Instruments and Methods in Physics Research Section A: Accelerators, Spectrometers, Detectors and Associated Equipment* **651**(1): 1–5.

Lisowski, P. W. and K. F. Schoenberg (2006). "The Los Alamos Neutron Science Center." *Nuclear Instruments & Methods in Physics Research. Section A, Accelerators, Spectrometers, Detectors and Associated Equipment* **562**(2): 910–914.

Long, A., S. Vogel (2022). "Energy Resolved Neutron Imaging (ERNI) at FP5." from https://lansce.lanl.gov/facilities/lujan/instruments/fp-5/index.php.

Losko, A. S. and S. C. Vogel (2022). "3D Isotope Density Measurements by Energy-Resolved Neutron Imaging." *Scientific Reports* **12**(1): 6648.

Mansy, M. S., I. I. Bashter, M. S. El-Mesiry, N. Habib and M. Adib (2015). "Filtered Epithermal Quasi-Monoenergetic Neutron Beams at Research Reactor Facilities." *Applied Radiation and Isotopes* **97**: 78–83.

Moreh, R., R. C. Block and Y. Danon (2006). "Generating a Multi-Line Neutron Beam Using an Electron Linac and a U-filter." *Nuclear Instruments and Methods in Physics Research Section A: Accelerators, Spectrometers, Detectors and Associated Equipment* **562**(1): 401–406.

Mosher, S. W., A. M. Bevill, S. R. Johnson, A. M. Ibrahim, C. R. Daily, T. M. Evans, J. C. Wagner, J. O. Johnson and R. E. Grove (2013). "ADVANTG—An Automated Variance Reduction Parameter Generator." Oak Ridge National Laboratory, Oak Ridge, TN. ORNL/TM-2013/416 Rev. 1.

Mosher, S. W. and S. C. Wilson (2018). "Algorithmic Improvements to MCNP5 for High-Resolution Fusion Neutronics Analyses." *Fusion Science and Technology* **74**(4): 263–276.

Mulligan, P. L., L. R. Cao and D. Turkoglu (2012). A Multi-Detector, Digitizer Based Neutron Depth Profiling Device for Characterizing Thin Film Materials. *Review of Scientific Instruments* **83**.

Rant, J. J. and M. Balaskó (2013). "Epithermal and Fast Neutron Radiography Using Photoluminescent Imaging Plates and Resonance and Threshold Activation Detectors." *The 12th International Conference of the Slovenian Society for Non-Destructive Testing, Portorož, Slovenia*: 251–260.

Rovira, G., A. Kimura, S. Nakamura, S. Endo, O. Iwamoto, N. Iwamoto, T. Katabuchi, K. Terada, Y. Kodama, H. Nakano, J.-i. Hori and Y. Shibahara (2021). "Neutron Beam Filter System for Fast Neutron Cross-Section Measurement at the ANNRI Beamline of MLF/J-PARC." *Nuclear Instruments and Methods in Physics Research Section A: Accelerators, Spectrometers, Detectors and Associated Equipment* **1003**: 165318.

Santodonato, L., H. Bilheux, B. Bailey, J. Bilheux, P. Nguyen, A. Tremsin, D. Selby and L. Walker (2015). "The CG-1D Neutron Imaging Beamline at the Oak Ridge National Laboratory High Flux Isotope Reactor." *Physics Procedia* **69**: 104–108.

Shinohara, T., T. Kai, K. Oikawa, T. Nakatani, M. Segawa, K. Hiroi, Y. Su, M. Ooi, M. Harada, H. Iikura, H. Hayashida, J. D. Parker, Y. Matsumoto, T. Kamiyama, H. Sato and Y. Kiyanagi (2020). "The Energy-Resolved Neutron Imaging System, RADEN." *Review of Scientific Instruments* **91**(4): 043302.

Tozser, S. (2009). "Full-Scale Reconstruction and Upgrade of the Budapest Research Reactor." *IAEA-TECDOC-1625*, IAEA.

Tremsin, A. S., S. C. Vogel, M. Mocko, M. A. M. Bourke, V. Yuan, R. O. Nelson, D. W. Brown and W. B. Feller (2013). "Energy Resolved Neutron Radiography at LANSCE Pulsed Neutron Facility." *Neutron News* **24**(4): 28–32.

Tremsin, A. S., S. C. Vogel, M. Mocko, M. A. M. Bourke, V. Yuan, R. O. Nelson, D. W. Brown and W. B. Feller (2013). "Non-Destructive Studies of Fuel Pellets by Neutron Resonance Absorption Radiography and Thermal Neutron Radiography." *Journal of Nuclear Materials* **440**(1): 633–646.

Tsang, F. Y. and R. M. Brugger (1976). "A Versatile Neutron Beam Filter Facility with Silicon and Iron Filters." *Nuclear Instruments and Methods* **134**(3): 441–447.

Vontobel, P., M. Tamaki, N. Mori, T. Ashida, L. Zanini, E. H. Lehmann and M. Jaggi (2006). "Post-Irradiation Analysis of SINQ Target Rods by Thermal Neutron Radiography." *Journal of Nuclear Materials* **356**(1): 162–167.

Willendrup, P. K. and K. Lefmann (2021). "McStas (ii): An Overview of Components, Their Use, and Advice for User Contributions." *Journal of Neutron Research* **23**: 7–27.

Xoubi, N. and R. T. Primm III (2005). "Modeling of the High Flux Isotope Reactor Cycle 400." Oak Ridge, TN, ORNL/TM-2004/251.

Zboray, R., R. Adams and Z. Kis (2017). "Fast Neutron Radiography and Tomography at a 10MW Research Reactor Beamline." *Applied Radiation and Isotopes* **119**: 43–50.